of target hydrazones **8a–h** in excellent yields. The structures of all title compounds were confirmed by their physical and spectral data, with overall yields in the range of 81–95%.[33]

All synthesized compounds were evaluated in vitro for their ability to inhibit the catalytic activity of PARG, and for comparison purposes, ADP-HPD was used as a positive control. PARG was isolated from rat testes and purified.[34] Its complementary DNA (cDNA) was cloned. Partial cDNA clones were joined to obtain a full length PARG DNAs and named recombinant protein G (RPG). The plasmids were transformed into *Escherichia coli*. The recombinant rat PARG protein was expressed as a glutathione S-transferase (GST) fusion protein, GST-RPG (136 kDa), and this was employed in the PARG activity assay[35] following the method described previously.[29,34] The [^{32}P]poly(ADP-ribose) used in the assay were prepared according to the method of Shimokawa et al.[36] The assay results are tabulated in Table 1. Certain of the compounds showed anti-PARG IC_{50} values in the low micromolar range. More specifically, compound **3d** (IC_{50}= 1.0 μM) was the most active PARG inhibitor. Compounds **3e**, **5d**, **5e**, **8a**, **8b** and **8c** were also potent inhibitors with IC_{50} values of 2.1, 3.1, 3.2, 3.1, 2.8 and 1.6 μM, respectively. It is noteworthy that terephthalic acid dihydrazide (having a 1,4 orientation about the central benzene ring) based trihydroxyphenyl regioisomers **3d–f** (IC_{50} values of 1.0, 2.1 and 9.9 μM, respectively) were found to be more efficacious than the isophthalic acid dihydrazide (having a 1,3 orientation about the central benzene ring) based trihydroxyphenyl regioisomers **5d–f** (IC_{50} values of 3.1, 3.2 and 18.8 μM, respectively). Dihydroxyphenyl derivatives were less potent as compared to their respective trihydroxyphenyl derivatives. The 2,3-, 2,4- and 3,4-dihydroxy and 2,4,6-trihydroxyphenyl derivatives analogous to **8a–h** were also prepared and evaluated. However, these compounds have not been reported, since they did not exhibit potent activity (IC_{50} >75 μM, Table 1). Among the tested trihydroxyphenyl regioisomers, the 2,3,4- and 3,4,5-trihydroxy isomers showed similar potencies, which were greater than for the 2,4,6-trihydroxy isomers.

The molecular docking analyses of the most potent compound **3d**, its regioisomer **5d** and the well studied PARG inhibitor ADP-HPD were carried out to infer critical interactions with the PARG active site. The X-ray crystal structure of rPARG^{385} was employed using the Molegro virtual docker. As depicted in Figure 2A–C, when **3d** and **5d** were docked into the deep central cleft of the catalytic domain, the most stable docking model of **3d** adopted a conformation that allows the C=O and C=N of one hydrazide group to participate in hydrogen bond interactions (bond length 2.76 Å and 3.08 Å, respectively) with the phenolic OH of Tyr791. In addition, the second hydrazide and phenol functional groups also potentially stabilize the conformation via formation of hydrogen-bonding interactions with Ala735, Glu752, Asn865 and Phe898. In contrast, the *meta*-regioisomer **5d** does not form hydrogen bond with Tyr791 and Glu752, although it forms several hydrogen bonds with other amino acid residues, including Asn736, His824, Asn865, Gly869, Ala870 and Phe871. Apparently, the *para*-orientation about the central benzene ring in compound **3d** endows it with the extended geometry required to be accommodated in the active site cleft. The docking conformation thus attained by **3d** in the rPARG catalytic domain is superior to its *meta*-regioisomer **5d** in respect to alignment and binding interactions. The docking orientations of **3d** and ADP-HPD within the binding site of the core macrodomain fold (residues 712–918) were highly similar (Fig. 2D).

In summary, we have designed and synthesized new phenolic hydrazide hydrazones, which were examined for their PARG inhibitory activity. Most of the synthesized compounds exhibited potent activity in an in vitro rPARG assay, with IC_{50} values in the low micromolar range. Molecular docking of the most potent compound **3d** identified its hypothetical binding mode within the rPARG catalytic domain. As per our preliminary finding, the phenolic hydrazide hydrazone functionality remarkably interacts with active site of PARG to inhibit its catalytic activity. This finding demonstrates that chemical modification and incorporation of this functionality in different biologically active scaffolds may lead to the development of more potent inhibitors of PARG enzyme. Currently, modification, synthesis and evaluation of PARG inhibitory activity are underway and the results will be reported in due course.

Acknowledgments

This study was supported by a Grant-in-Aid for Cancer Research from the Ministry of Health and Welfare of Japan (11104962). We thank Prof. Tomohisa Nagamatsu, Department of Medical Technology, Kumamoto Health Science University, Japan; Miss. Hiromi Harada, National Cancer Center Research Institute, Japan, and Dr. Yoshinobu Ishikawa, School of Pharmaceutical Sciences, University of Shizuoka, Japan for their assistances.

Supplementary data

Supplementary data associated with this article can be found, in the online version, at http://dx.doi.org/10.1016/j.bmcl.2014.06.065. These data include MOL files and InChiKeys of the most important compounds described in this article.

References and notes

1. Diefenbach, J.; Burkle, A. *Cell. Mol. Life Sci.* **2005**, *62*, 721.
2. D'Amours, D.; Desnoyers, S.; D'Silva, I.; Poirier, G. G. *Biochem. J.* **1999**, *342*, 249.
3. Schreiber, V.; Dantzer, F.; Ame, J. C.; de Murcia, G. *Nat. Rev. Mol. Cell Biol.* **2006**, *7*, 517.
4. Rulten, S. L.; Fisher, A. E. O.; Robert, I.; Zuma, M. C.; Rouleau, M.; Ju, L.; Poirier, G.; Reina-San-Martin, B.; Caldecott, K. W. *Mol. Cell* **2011**, *41*, 33.
5. Davidovic, L.; Vodenicharov, M.; Affar, E. B.; Poirier, G. G. *Exp. Cell Res.* **2001**, *268*, 7.
6. Murai, J.; Huang, S. Y.; Das, B. B.; Renaud, A.; Zhang, Y.; Doroshow, J. H.; Ji, J.; Takeda, S.; Pommier, Y. *Cancer Res.* **2012**, *72*, 5588.
7. Yu, S. W.; Wang, H.; Poitras, M. F.; Coombs, C.; Bowers, W. J.; Federoff, H. J.; Poirier, G. G.; Dawson, T. M.; Dawson, V. L. *Science* **2002**, *297*, 259.
8. Shirai, H.; Poetsch, A. R.; Gunji, A.; Maeda, D.; Fujimori, H.; Fujihara, H.; Yoshida, T.; Ogino, H.; Masutani, M. *Cell Death Dis.* **2013**, *4*, e656.
9. Nakadate, Y.; Kodera, Y.; Kitamura, Y.; Tachibana, T.; Tamura, T.; Koizumi, F. *Biochem. Biophys. Res. Commun.* **2013**, *441*, 793.
10. Zhou, Y.; Feng, X.; Koh, D. W. *Biochemistry* **2011**, *50*, 2850.
11. Ying, W.; Sevigny, M. B.; Chen, Y.; Swanson, R. A. *Proc. Natl. Acad. Sci. U.S.A.* **2001**, *98*, 12227.
12. Blenn, C.; Wyrsch, P.; Bader, J.; Bollhalder, M.; Althaus, F. R. *Cell. Mol. Life Sci.* **2011**, *68*, 1455.
13. Shen, Y.; Rehman, F. L.; Feng, Y.; Boshuizen, J.; Bajrami, I.; Elliott, R.; Wang, B.; Lord, C. J.; Post, L. E.; Ashworth, A. *Clin. Cancer Res.* **2013**, *19*, 5003.
14. O'Sullivan, C. C.; Moon, D. H.; Kohn, E. C.; Lee, J.-M. *Front. Oncol.* **2014**, *4*, 42.
15. Kummar, S.; Chen, A.; Parchment, R. E.; Kinders, R. J.; Ji, J.; Tomaszewski, J. E.; Doroshow, J. H. *BMC Med.* **2012**, *10*, 25.
16. Slade, D.; Dunstan, M. S.; Barkauskaite, E.; Weston, R.; Lafite, P.; Dixon, N.; Ahel, M.; Leys, D.; Ahel, I. *Nature* **2011**, *477*, 616.
17. Dunstan, M. S.; Barkauskaite, E.; Lafite, P.; Knezevic, C. E.; Brassington, A.; Ahel, M.; Hergenrother, P. J.; Leys, D.; Ahel, I. *Nat. Commun.* **2012**, *3*, 878.
18. Kim, I.-K.; Kiefer, J. R.; Ho, C. M. W.; Stegeman, R. A.; Classen, S.; Tainer, J. A.; Ellenberger, T. *Nat. Struct. Mol. Biol.* **2012**, *19*, 653.
19. Tucker, J. A.; Bennett, N.; Brassington, C.; Durant, S. T.; Hassall, G.; Holdgate, G.; McAlister, M.; Nissink, J. W. M.; Truman, C.; Watson, M. *PLoS ONE* **2012**, *7*, e50889.
20. Patel, C. N.; Koh, D. W.; Jacobson, M. K.; Oliveira, M. A. *Biochem. J.* **2005**, *388*, 493.
21. Koh, D. W.; Patel, C. N.; Ramsinghani, S.; Slama, J. T.; Oliveira, M. A.; Jacobson, M. K. *Biochemistry* **2003**, *42*, 4855.
22. Hatakeyama, K.; Nemoto, Y.; Ueda, K.; Hayaishi, O. *J. Biol. Chem.* **1986**, *261*, 14902.
23. Tanuma, S.; Sakagami, H.; Endo, H. *Biochem. Int.* **1989**, *18*, 701.
24. Tavassoli, M.; Tavassoli, M. H.; Shall, S. *Biochim. Biophys. Acta* **1985**, *827*, 228.
25. Slama, J. T.; Aboul-Ela, N.; Goli, D. M.; Cheesman, B. V.; Simmons, A. M.; Jacobson, M. K. *J. Med. Chem.* **1995**, *38*, 389.
26. Slama, J. T.; Aboul-Ela, N.; Jacobson, M. K. *J. Med. Chem.* **1995**, *38*, 4332.

27. Formentini, L.; Arapistas, P.; Pittelli, M.; Jacomelli, M.; Pitozzi, V.; Menichetti, S.; Romani, A.; Giovannelli, L.; Moroni, F.; Chiarugi, A. *Br. J. Pharmacol.* **2008**, *155*, 1235.
28. Finch, K. E.; Knezevic, C. E.; Nottbohm, A. C.; Partlow, K. C.; Hergenrother, P. J. *ACS Chem. Biol.* **2012**, *7*, 563.
29. Steffen, J. D.; Coyle, D. L.; Damodaran, K.; Beroza, P.; Jacobson, M. K. *J. Med. Chem.* **2011**, *54*, 5403.
30. Blenn, C.; Wyrsch, P.; Althaus, F. R. *Molecules* **1854**, *2011*, 16.
31. Falsig, J.; Christiansen, S. H.; Feuerhahn, S.; Bürkle, A.; Oei, S. L.; Keil, C.; Leist, M. *Eur. J. Pharmacol.* **2004**, *497*, 7.
32. Labieniec, M.; Gabryelak, T.; Falcioni, G. *Mutat. Res.* **2003**, *539*, 19.
33. *General procedure for the synthesis of compounds **3a–f**, **5a–f** and **8a–h**:* A mixture of an appropriate dihydrazide (1 mmol), an appropriate hydroxybenzaldehyde (2 mmol) and acetic acid (2/3 drops) in methanol (25 ml) was heated under reflux with stirring for 6–8 h. Then the reaction mixture was cooled with stirring. Precipitated solid was collected by filtration, and washed with little ethanol and hexane to give the target products **3a–f**, **5a–f** and **8a–h.** Compound **3a**: Off-white solid; yield: 92%; mp: >300 °C; ^{1}H NMR (300 MHz, DMSO-d_6): δ 6.75 (t, J = 7.8 Hz, 2H), 6.87 (d, J = 7.8 Hz, 2H), 6.99 (d, J = 7.7 Hz, 2H), 8.09 (s, 4H), 8.64 (s, 2H), 9.25 (s, 2H), 11.04 (s, 2H), 12.24 (s, 2H); TOF MS: calcd for $C_{22}H_{19}N_4O_6$ $[M+H]^+$ 435.13, found 435.14. Compound **3b**: Yellow solid; yield: 86%; mp: >300 °C; ^{1}H NMR (300 MHz, DMSO-d_6): δ 6.33–6.38 (m, 4H), 7.33 (d, J = 8.4 Hz, 2H), 8.05 (s, 4H), 8.53 (s, 2H), 9.96 (br s, 2H), 11.40 (br s, 2H), 12.02 (br s, 2H); TOF MS: calcd for $C_{22}H_{19}N_4O_6$ $[M+H]^+$ 435.13, found 435.15. Compound **3c**: Yellow solid; yield: 89%; mp: >300 °C; ^{1}H NMR (300 MHz, DMSO-d_6): δ 6.79 (d, J = 8.1 Hz, 2H), 6.94 (d, J = 8.1 Hz, 2H), 7.26 (s, 2H), 8.02 (s, 4H), 8.28 (s, 2H), 9.34 (br s, 4H), 11.72 (br s, 2H); TOF MS: calcd for $C_{22}H_{19}N_4O_6$ $[M+H]^+$ 435.13, found 435.25. Compound **3d**: Off-white solid; yield: 95%; mp: >300 °C; ^{1}H NMR (300 MHz, DMSO-d_6): δ 6.40 (d, J = 8.4 Hz, 2H), 6.80 (d, J = 8.4 Hz, 2H), 8.06 (s, 4H), 8.50 (s, 4H), 9.50 (s, 2H), 11.44 (s, 2H), 12.08 (s, 2H); TOF MS: calcd for $C_{22}H_{19}N_4O_8$ $[M+H]^+$ 467.12, found 467.23. Compound **3e**: Yellow solid; yield: 88%; mp: >300 °C; ^{1}H NMR (300 MHz, DMSO-d_6): δ 6.71 (s, 4H), 8.01 (s, 4H), 8.19 (s, 2H), 8.66 (br s, 2H), 9.13 (br s, 4H), 11.69 (br s, 2H); TOF MS: calcd for $C_{22}H_{19}N_4O_8$ $[M+H]^+$ 467.12, found 467.22. Compound **3f**: Orange solid; yield: 83%; mp: >300 °C; ^{1}H NMR (300 MHz, DMSO-d_6): δ 5.85 (s, 4H), 8.04 (s, 4H), 8.82 (s, 2H), 9.86 (s, 2H), 11.09 (s, 4H), 12.01 (s, 2H); TOF MS: calcd for $C_{22}H_{19}N_4O_8$ $[M+H]^+$ 467.12, found 467.20. Compound **5a:** Off-white solid; yield: 91%; mp: >300 °C; ^{1}H NMR (300 MHz, DMSO-d_6): δ 6.75 (t, J = 7.8 Hz, 2H), 6.87 (d, J = 7.7 Hz, 2H), 6.99 (d, J = 7.7 Hz, 2H), 7.73 (t, J = 7.7 Hz, 1H), 8.16 (d, J = 7.7 Hz, 2H), 8.53 (s, 1H), 8.64 (s, 2H), 9.25 (s, 2H), 11.07 (s, 2H), 12.28 (s, 2H); TOF MS: calcd for $C_{22}H_{19}N_4O_6$ $[M+H]^+$ 435.13, found 435.22. Compound **5b**: Off-white solid; yield: 87%; mp: >300 °C; ^{1}H NMR (300 MHz, DMSO-d_6): δ 6.33–6.39 (m, 4H), 7.33 (d, J = 8.4 Hz, 2H), 7.69 (t, J = 7.7 Hz, 1H), 8.11 (d, J = 7.7 Hz, 2H), 8.47 (s, 1H), 8.54 (s, 2H), 9.98 (s, 2H), 11.42 (s, 2H), 12.08 (s, 2H); TOF MS: calcd for $C_{22}H_{19}N_4O_6$ $[M+H]^+$ 435.13, found 435.24. Compound **5c**: Off-white solid; yield: 90%; mp: >300 °C; ^{1}H NMR (300 MHz, DMSO-d_6): δ 6.79 (d, J = 7.9 Hz, 2H), 6.94 (d, J = 7.9 Hz, 2H), 7.26 (s, 2H), 7.65 (t, J = 7.7 Hz, 1H), 8.07 (d, J = 7.7 Hz, 2H), 8.28 (s, 2H), 8.42 (s, 1H), 9.35 (br s, 4H), 11.74 (br s, 2H); TOF MS: calcd for $C_{22}H_{19}N_4O_6$ $[M+H]^+$ 435.13, found 435.24. Compound **5d**: off-white solid; yield: 93%; mp: >300 °C; ^{1}H NMR (300 MHz, DMSO-d_6): δ 6.39 (d, J = 8.4 Hz, 2H), 6.80 (d, J = 8.4 Hz, 2H), 7.70 (t, J = 7.8 Hz, 1H), 8.13 (d, J = 7.5 Hz, 2H), 8.50 (s, 5H), 9.47 (s, 2H), 11.47 (s, 2H), 12.11 (s, 2H); TOF MS: calcd for $C_{22}H_{19}N_4O_8$ $[M+H]^+$ 467.12, found 467.23. Compound **5e**: Off-white solid; yield: 89%; mp: >300 °C; ^{1}H NMR (300 MHz, DMSO-d_6): δ 6.70 (br s, 4H), 7.67 (s, 1H), 8.07 (s, 2H), 8.19 (s, 2H), 8.40 (s, 1H), 8.62 (br s, 2H), 9.15 (br s, 4H), 11.72 (br s, 2H); TOF MS: calcd for $C_{22}H_{19}N_4O_8$ $[M+H]^+$ 467.12, found 467.20. Compound **5f**: brown solid; yield: 86%; mp: >300 °C; ^{1}H NMR (300 MHz, DMSO-d_6): δ 5.84 (s, 4H), 7.67 (t, J = 7.7 Hz, 1H), 8.09 (d, J = 7.7 Hz, 2H), 8.48 (s, 1H), 8.83 (s, 2H), 9.83 (s, 2H), 11.09 (br s, 4H), 12.05 (s, 2H); TOF MS: calcd for $C_{22}H_{19}N_4O_8$ $[M+H]^+$ 467.12, found 467.18. Compound **8a**: yellow solid; yield: 88%; mp: >300 °C; δ 6.39 (d, J = 8.4 Hz, 2H), 6.77 (d, J = 8.4 Hz, 2H), 8.53 (br s, 2H), 8.62 (s, 2H), 9.59 (br s, 2H), 11.27 (br s, 2H), 12.53 (br s, 2H); TOF MS: calcd for $C_{16}H_{15}N_4O_8$ $[M+H]^+$ 391.09, found 391.30. Compound **8b**: Yellow solid; yield: 86%; mp: >300 °C; ^{1}H NMR (300 MHz, DMSO-d_6): δ 6.67 (s, 4H), 8.31 (s, 2H), 8.64 (s, 2H), 9.15 (s, 4H), 11.98 (s, 2H); TOF MS: calcd for $C_{16}H_{15}N_4O_8$ $[M+H]^+$ 391.09, found 391.28. Compound **8c**: Brown solid; yield: 85%; mp: 239–240 °C (decomp.); ^{1}H NMR (300 MHz, DMSO-d_6): δ 3.27 (s, 1H), 3.55 (s, 1H), 6.25 (d, J = 8.4 Hz, 1H), 6.37 (d, J = 8.4 Hz, 1H), 6.78 (d, J = 8.6 Hz, 1H), 6.91 (d, J = 8.6 Hz, 1H), 8.13 (s, 1H), 8.23 (s, 1H), 8.48 (br s, 2H), 9.44 (br s, 3H), 11.25 (br s, 2H), 11.69 (br s, 1H); TOF MS: calcd for $C_{17}H_{17}N_4O_8$ $[M+H]^+$ 405.10, found 405.30. Compound **8d**: brown solid; yield: 83%; mp: 201–202 °C; ^{1}H NMR (300 MHz, DMSO-d_6): δ 3.55 (s, 1H), 3.87 (s, 1H), 6.54–6.64 (m, 4H), 7.72 (s, 1H), 7.89 (s, 1H), 8.89 (br s, 6H), 11.22 (br s, 2H); TOF MS: calcd for $C_{17}H_{17}N_4O_8$ $[M+H]^+$ 405.10, found 405.25. Compound **8e**: Pale yellow solid; yield: 89%; mp: 283–284 °C (decomp.); ^{1}H NMR (300 MHz, DMSO-d_6): δ 2.44 (br s, 4H), 6.31 (d, J = 8.4 Hz, 2H), 6.69 (d, J = 8.4 Hz, 2H), 8.12 (s, 2H), 8.39 (s, 2H), 9.36 (s, 2H), 11.31 (s, 2H), 11.49 (s, 2H); TOF MS: calcd for $C_{18}H_{19}N_4O_8$ $[M+H]^+$ 419.12, found 419.31. Compound **8f**: Pale yellow solid; yield: 84%; mp: 243–244 °C; ^{1}H NMR (300 MHz, DMSO-d_6): δ 2.88 (br s, 4H), 6.61 (s, 4H), 7.72 (s, 1H), 7.86 (s, 1H), 8.49 (br s, 2H), 9.07 (br s, 4H), 10.97 (s, 1H), 11.13 (s, 1H); TOF MS: calcd for $C_{18}H_{19}N_4O_8$ $[M+H]^+$ 419.12, found 419.33. Compound **8g**: Pale yellow solid; yield: 85%; mp: 262–263 °C; ^{1}H NMR (300 MHz, DMSO-d_6): δ 1.88 (br s, 2H), 2.21–2.27 (m, 2H), 2.64 (br s, 2H), 6.35 (d, J = 8.4 Hz, 2H), 6.72 (d, J = 8.4 Hz, 2H), 8.15 (s, 2H), 8.43 (br s, 2H), 9.40 (br s, 2H), 11.46 (br s, 4H); TOF MS: calcd for $C_{19}H_{21}N_4O_8$ $[M+H]^+$ 433.14, found 433.27. Compound **8h**: Pale yellow solid; yield: 81%; mp: 174–175 °C; ^{1}H NMR (300 MHz, DMSO-d_6): δ 1.85 (br s, 2H), 2.16–2.22 (m, 2H), 2.61–2.66 (m, 2H), 6.57 (s, 2H), 6.61 (s, 2H), 7.69 (s, 1H), 7.85 (s, 1H), 8.50 (br s, 2H), 9.06 (br s, 4H), 10.90 (s, 1H), 11.06 (s, 1H); TOF MS: calcd for $C_{19}H_{21}N_4O_8$ $[M+H]^+$ 433.14, found 433.16.
34. Shimokawa, T.; Masutani, M.; Nagasawa, S.; Nozaki, T.; Ikota, N.; Aoki, Y.; Nakagama, H.; Sugimura, T. *J. Biochem.* **1999**, *126*, 748.
35. The sample solutions in DMSO were added to 4 μM [^{32}P]poly(ADP-ribose) in 20 mM potassium phosphate buffer (pH 7.5), 50 mL KCl and 10 mM 2-mercaptoethanol. The reaction was initiated by the addition of 20 μL of GST-PARG (15 ng), and the reaction mixture was incubated at 37 °C for 30 min. The reaction was terminated by the addition of SDS to be final concentration of 1%. Next, 2 μL of the reaction mixture was spotted on a poly(ethyleneimine) cellulose TLC plate (Macherey-Nagel Co.), and the plate was developed with 0.1 M LiCl, 3 M AcOH and 3 M urea. Then, the radioactivity of the spots was analyzed with photosensitive Fuji imaging plate BAS-2500 (Fuji Film). The proportion of degradation products to the whole was measured, and PARG activity was calculated.
36. Shimokawa, T.; Ogino, H.; Maeda, D.; Nakagama, H.; Sugimura, T.; Masutani, M. *Org. Chem. Insights* **2009**, *2*, 1.

Molecular Genetics and Metabolism Reports 1 (2014) 391–400

Contents lists available at ScienceDirect

Molecular Genetics and Metabolism Reports

journal homepage: http://www.journals.elsevier.com/molecular-genetics-and-metabolism-reports/

Effects of intracerebroventricular administration of 2-hydroxypropyl-β-cyclodextrin in a patient with Niemann–Pick Type C disease

Muneaki Matsuo [a,*], Koki Shraishi [c], Koki Wada [d], Yoichi Ishitsuka [c], Hirohito Doi [a], Miyuki Maeda [b], Tatsuhiro Mizoguchi [a], Junya Eto [a], Sakiko Mochinaga [b], Hidetoshi Arima [c], Tetsumi Irie [c]

[a] *Department of Pediatrics, Saga University, Faculty of Medicine, Saga, Japan*
[b] *Department of Pharmacology, Saga University, Faculty of Medicine, Saga, Japan*
[c] *Graduate School of Pharmaceutical Sciences, Kumamoto University, Kumamoto, Japan*
[d] *Research Institute, Nihon Shokuhin Kako Co., Ltd, Japan*

ARTICLE INFO

Article history:
Received 14 July 2014
Received in revised form 19 August 2014
Accepted 19 August 2014
Available online xxxx

Keywords:
Niemann–Pick Type C disease
Cyclodextrin
Cholesterol
Intrathecal administration
Intracerebroventricular administration
Pharmacokinetics

ABSTRACT

Niemann–Pick Type C disease (NPC) is an autosomal recessive lysosomal storage disorder characterized by progressive neurological deterioration. Previously, we reported that intravenous administration of 2-hydroxypropyl-β-cyclodextrin (HPB-CD) in two patients with NPC had only partial and transient beneficial effects on neurological function. The most likely reason for HPB-CD not significantly improving the neurological deficits of NPC is its inability to cross the blood–brain barrier. Herein, we describe the effects of intrathecal HPB-CD in an eight-year-old patient with a perinatal onset of NPC, administered initially at a dose of 10 mg/kg every other week and increased up to 10 mg/kg twice a week. Clinically, the patient maintained residual neurological functions for two years, at which time nuclear magnetic resonance spectroscopy showed a decreased choline to creatine ratio and increased N-acetylaspartate to creatine ratio, and positron emission tomography revealed increased standardized uptake values. Total-tau in the cerebrospinal fluid (CSF) was also decreased after two years. No adverse effects were observed over the course of treatment. The CSF concentrations of HPB-CD during the distribution phase after the injections were comparable with those at which HPB-CD could normalize cellular cholesterol

Abbreviations: NPC, Niemann–Pick Type C disease; HPB-CD, 2-hydroxypropyl-β-cyclodextrin; CD, cyclodextrin; MRS, nuclear magnetic resonance spectroscopy; NAA, N-acetylaspartate; Cho, choline; Cr, creatine; PET, positron emission tomography; CSF, cerebrospinal fluid.

* Corresponding author at: Department of Pediatrics, Saga University, Faculty of Medicine, 5-1-1, Nabeshima, Saga 849-8501, Japan. Fax: +81 952 34 2064.
E-mail address: matsuo@cc.saga-u.ac.jp (M. Matsuo).

http://dx.doi.org/10.1016/j.ymgmr.2014.08.004

abnormality in vitro. Further studies are necessary to elucidate the mechanisms of action of HPB-CD in NPC, and to determine the optimal dose and intervals of HPB-CD injection.

1. Introduction

Niemann–Pick Type C disease (NPC) is an autosomal recessive lysosomal storage disorder characterized by progressive neurological deterioration. NPC is caused by mutations in either the *NPC1* or *NPC2* gene, both of which encode proteins involved in regulating intracellular lipid trafficking. These gene mutations lead to marked lysosomal accumulation of unesterified cholesterol and several glycosphingolipids [1].

Recent studies in NPC mice showed that hydroxypropyl-β-cyclodextrin (HPB-CD) injections are effective in treating the disease [2–5]. Cyclodextrins (CDs) are cyclic oligosaccharides known as host molecules that form inclusion complexes with guest molecules, including exogenous and endogenous lipophiles, and are widely used in food, cosmetics, and pharmaceuticals [6]. HPB-CD has high aqueous solubility and extremely low toxicity, and is already used clinically with other drugs in parenteral preparations. Previously, we reported the effectiveness of HPB-CD administered intravenously in two patients with NPC [7]. It had only partial and transient beneficial effects on neurological function, probably due to issues with crossing the blood–brain barrier [4]. Recently, direct administration of HPB-CD into the cerebral ventricle of NPC model mice normalized the biochemical abnormalities and completely prevented the expected neurodegeneration, and Phase I Clinical Trial of intracerebroventricular (ICV) HPB-CD administration began in February 2013 [4,8]. Thus, we tested the effectiveness and safety of intrathecal administration of HPB-CD in a patient with NPC.

2. Patient and methods

2.1. Patient

A girl in whom hepatosplenomegaly was detected before birth, was diagnosed with NPC based on mutations in the *NPC1* gene (c.581_592delinsG, Y1088C) at the age of two months. She developed slowly until 3 years of age, walking alone at 19 months and using two-word sentences at 3 years. However, after 3 years of age she started to exhibit rapid neurological deterioration, including progressive ataxia, cataplexy, dysarthria, dysphagia, and convulsions. She was started on intravenous HPB-CD treatment at 4 years of age, by which stage she had marked hepatosplenomegaly, could walk indoors with assistance, and speak only a few unclear words. She also exhibited vertical gaze palsy, mild occasional dysphagia, slight hypotonia, ataxia, frequent attacks of cataplexy, and rare convulsions. After one year of treatment with HPB-CD, the hepatosplenomegaly was slightly improved, but unfortunately, her neurological signs had worsened as she gradually developed dysphagia, rigidity, and frequent seizures. Consequently, she became bed-ridden and lost the ability to speak. She was started on tube feeding via a gastrostomy. We added miglustat after one year of treatment with HPB-CD; however, her neurological deterioration continued. Her swallowing function worsened, and she suffered from severe aspiration pneumonia. Her head MRI also showed progressive brain atrophy (Fig. 2).

2.2. Intrathecal administration of HPB-CD

After two years of intravenous HPB-CD treatment, intrathecal HPB-CD therapy was started at the age of 6 years. With informed consent from the parents, we initiated a 10 mg/kg dose of 20% HPB-CD diluted with 6 mL saline administered via lumber puncture every other week. Two months later, no adverse effects were observed, thus we implanted an Ommaya reservoir to administer 20 mg/kg HPB-CD weekly thereafter (Table 1). The dose was increased by up to 450 mg (22.5 mg/kg) every week. Fifteen months later, we changed the treatment schedule to a 200-mg dose twice a week according to the measured concentrations of HPB-CD in the cerebrospinal fluid (CSF) (Table. 2). Twenty-one months later, we transiently increased the dose of HPB-CD up to 300 mg twice a week, but reduced it again shortly after due to an increased total tau in the CSF. Intravenous administration of HPB-CD was stopped 12 months after the start of intrathecal HPB-CD

Table 1
The dose and intervals of HPB-CD.

	IV HPB-CD	ICV HPB-CD	Interval	Weight
0–2 M	20 g × 2/week	165 mg	Every 2 weeks	16.5 kg
3 M–4 M	20 g × 2/week	330 mg	Every 2 weeks	15.7 kg
5 M–6 M	20 g × 2/week	450 mg	Every 2 weeks	18.5 kg
7 M–14 M	20 g × 1/week	450 mg	Every week	20.0 kg
15 M–20 M		200 mg	Twice a week	21.3 kg
21 M–22 M		300 mg	Twice a week	22.4 kg
23 M–		200 mg	Twice a week	24.0 kg

treatment, whereas miglustat was continued. The treatment protocol used in the present study was approved by the Ethics Committees of Saga University (no. 2009-05-04) and Kumamoto University (no. 608).

Clinical assessments were performed before the start of treatment and then after 3, 6, 12, 18, and 24 months of treatment, comprising blood and CSF testing, head magnetic resonance imaging (MRI), magnetic resonance spectroscopy (MRS), positron emission tomography (PET), electroencephalography (EEG), auditory brainstem evoked potentials (ABR), and videofluoroscopy. CSF levels of total tau (T-tau) were also measured by the ELISA Kit (R&D, Minneapolis) according to the manufacture's protocol to determine axonal damage.

2.3. Determination of HPB-CD concentrations in CSF

CSF concentrations of HPB-CD were determined by high-performance liquid chromatography according to the method of Frijlink et al. [9] with slight modifications. HPB-CD was purchased from Roquette Japan K.K. (Osaka). The average degree of substitution of 2-hydroxypropyl groups was 4.41, and the average molecular weight was 1391 Da. All other chemicals used were of analytical grade.

The HPLC system consisted of two LC-10A pumps (Shimadzu, Tokyo), a SIL-10A XL auto injector (Shimadzu), and a SPD-10A UV–VIS absorbance detector (Shimadzu). Capillary tubing of 10 m (1.0 mm i.d.) was used for mixing the column eluent with the post-column reagent.

We added 100 μL of CSF sample to 40 μL of 20% trichloroacetic acid. After mixing and centrifugation at 10,000 *g* at 4 °C for 5 min, 40 μL of 1 M sodium carbonate solution was added to 80 μL of the clear supernatant. The sample was passed through a filter (MILLEX-HP PES 0.45 μm), and 10 μL of the filtrate was injected onto the HPLC column. The analytical column was a OHpak Shodex column (SHOWA DENKO K.K., Tokyo, 300 × 8.0 mm i.d.), used with a guard column. The column eluent was a sodium chloride solution (0.9%) adjusted to pH 4.3 by acetic acid, with a flow rate of 0.9 mL/min. The post-column reagent was 8 mM sodium carbonate and 60 μM phenolphthalein in water, and the flow rate was 0.9 mL/min. The effluent was monitored at 546 nm. The detection limit of HPB-CD in CSF was 20 μg/mL.

3. Results

3.1. Clinical symptoms and signs

Clinical symptoms and signs remained virtually stable during two years of intracerebroventricular HPB-CD treatment. Although the patient's facial expression is slightly impaired two years later, she can still laugh with

Table 2
Concentrations of HPB-CD in the CSF after the intrathecal injection of HPB-CD at a dose of 200 mg or 300 mg to the patient with NPC.

Age of the patient (year)	Body weight of the patient (kg)	Dose of HPB-CD (mg)	Concentration of HPB-CD in the CSF[a] (μg/mL)		Apparent volume of distribution[b] (mL/kg)
			15 min after injection	1 h after injection	
7.58	20.1	200	1106 ± 24	205 ± 23	5.1
7.75	23.1	300	2122 ± 28	284 ± 25	3.1

[a] The mean ± S.E.M. of three determinations of the same sample.
[b] Estimated by the dose of HPB-CD and the CSF concentration extrapolated immediately after the injection.

voice and horizontal eye movements have been preserved. Swallowing function assessed by videofluoroscopy was slightly improved at 18 months after treatment started, but became slightly worse at 24 months (Supplemental data 1). At 21 months from the beginning of intrathecal HPB-CD, she received the SynchroMed-2 pump implant to start intrathecal baclofen (ITB) therapy for increased rigospasticity of her trunk and limbs. She suffered from aspiration pneumonia immediately after the implantation operation. Seizure frequency was not changed significantly.

Frontal dominant, irregular, high-voltage, slow activities on the awake EEG were significantly decreased after two years of treatment with intrathecal HPB-CD (Fig. 1), although there were no significant changes on brain MRI (Fig. 2). MRS of the cerebral white matter, basal ganglia, and cerebellum showed a decreased choline to creatine ratio (Cho/Cr), indicating decreased myelin destruction, and an increase in the N-acetylaspartate to creatine ratio (NAA/Cr), indicating decreased neuronal and axonal damage in all areas (Fig. 3A,B). The standardized uptake values on PET were slightly increased in all areas after two years (Fig. 4A, B), indicating increased metabolism and activities of the patient's brain. There were no changes in ABR.

3.2. Changes in CSF T-tau

Changes in CSF T-tau are represented in Fig. 5. The levels of CSF T-tau gradually decreased after the beginning of intrathecal HPB-CD therapy, but were transiently increased from the 21 months to 23 months period, when the dose of HPB-CD reached 300 mg twice a week.

3.3. HPB-CD concentrations in CSF

Table 1 details the concentrations of HPB-CD in CSF 15 min and 1 h after the intrathecal injection of HPB-CD at a dose of 200 mg (10.0 mg/kg) or 300 mg (13.0 mg/kg). At these doses, the HPB-CD concentration ranged from 2122 μg/mL (1.53 mM) to 205 μg/mL (0.15 mM) during 1 h. The apparent volumes of distribution for HPB-CD were estimated to be 5.1 mL/kg at a dose of 200 mg and 3.1 mL/kg at a dose of 300 mg, respectively.

4. Discussion

Intravenous HPB-CD treatment has only partial and transient beneficial effects on neurological function, whereas direct administration of HPB-CD into the cerebral ventricle of NPC model mice normalizes the biochemical abnormalities and completely prevents the expected neurodegeneration [4]. Herein, we also demonstrated the efficacy of ICV administration of HPB-CD in a patient with NPC. Unfortunately, it was difficult to improve the clinical symptoms because our patient was already progressed at the beginning of ICV HPB-CD therapy. However, she could maintain residual functions such as horizontal gaze pursuit and laughing with voice, and swallowing function at 18 months was improved. Taking into account the rapid progression of neurological dysfunction in our patient after two years of treatment with intravenous HPB-CD and miglustat, the stable clinical state for two years with ICV HPB-CD indicates the effectiveness of such therapy. Furthermore, EEG, MRS and PET study showed beneficial effects.

Increased levels of T-tau in CSF have been reported in NPC patient [10,11], indicating axonal degeneration. The CSF T-tau levels of our patient were decreased, except for one transient increase at 20 to 22 months after the beginning of ICV HPB-CD therapy. Interestingly, the reduced levels of NAA/Cr in MRS, which indicates degeneration of neurons and axons, changed reciprocally with the CSF T-tau levels. Although increased NAA/Cr and reduced T-tau have been reported in miglustat therapy, ICV HPB-CD was probably the major effective contributor to improvements in this case because miglustat had been started one year before the beginning of the ICV HPB-CD and the patient's neurological conditions deteriorated during the pre-ICV HPB-CD period.

The major concern with direct administration of HPB-CD into CSF is adverse effects, especially in auditory function, and dose-dependent auditory toxicity from HPB-CD has been reported in cats [12]. Specifically, weekly subcutaneous injections of 4 g/kg HPB-CD and every other weekly intrathecal injections of 120 mg HPB-CD in NPC cats increased the hearing threshold. Fortunately, our patient showed no adverse

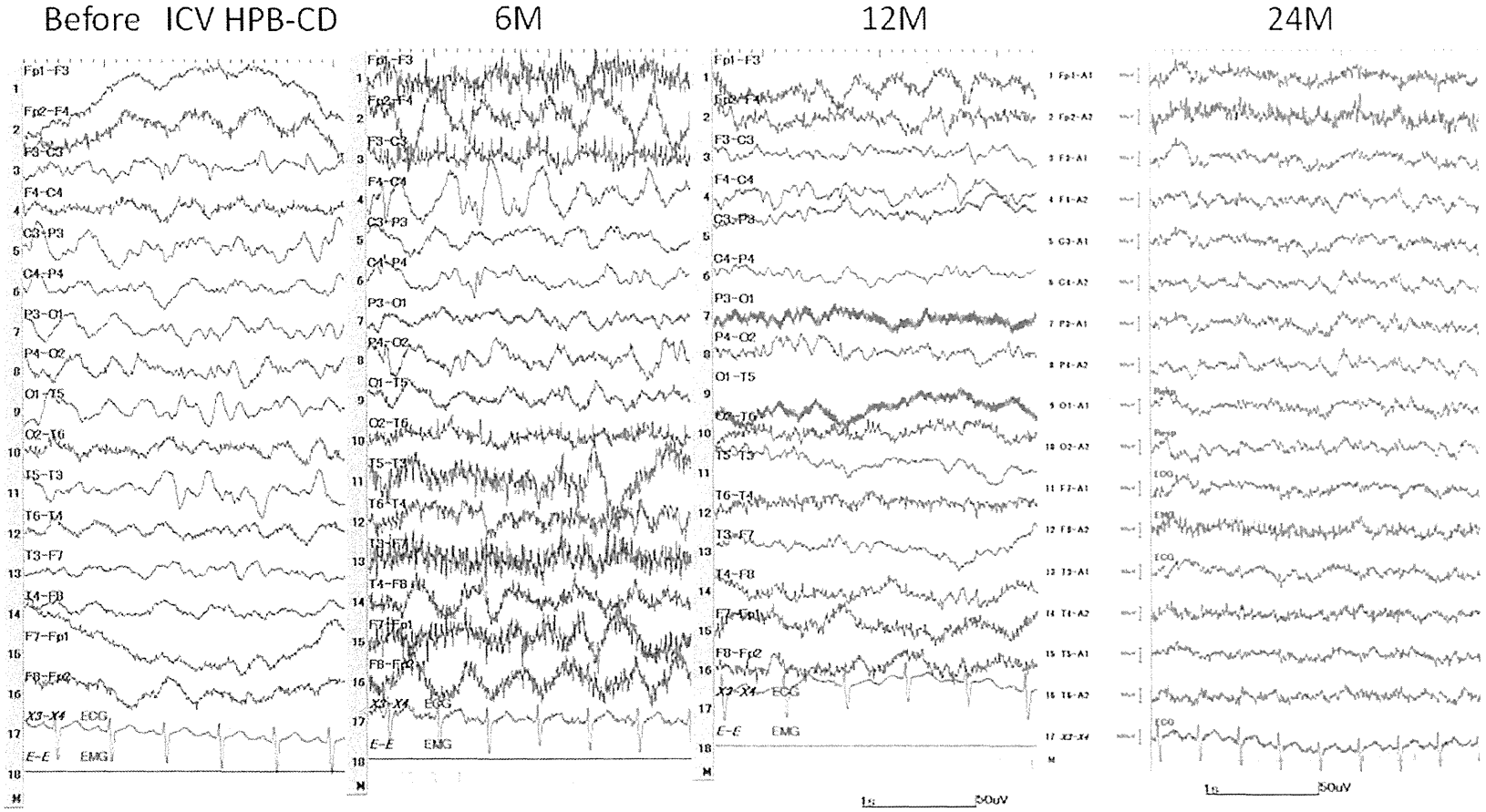

Fig. 1. Changes in the awake EEG before and after treatment with intrathecal 2-hydroxypropyl-β-cyclodextrin. Frontal-predominant, irregular, high-voltage, slow activities were significantly decreased after two years of treatment.

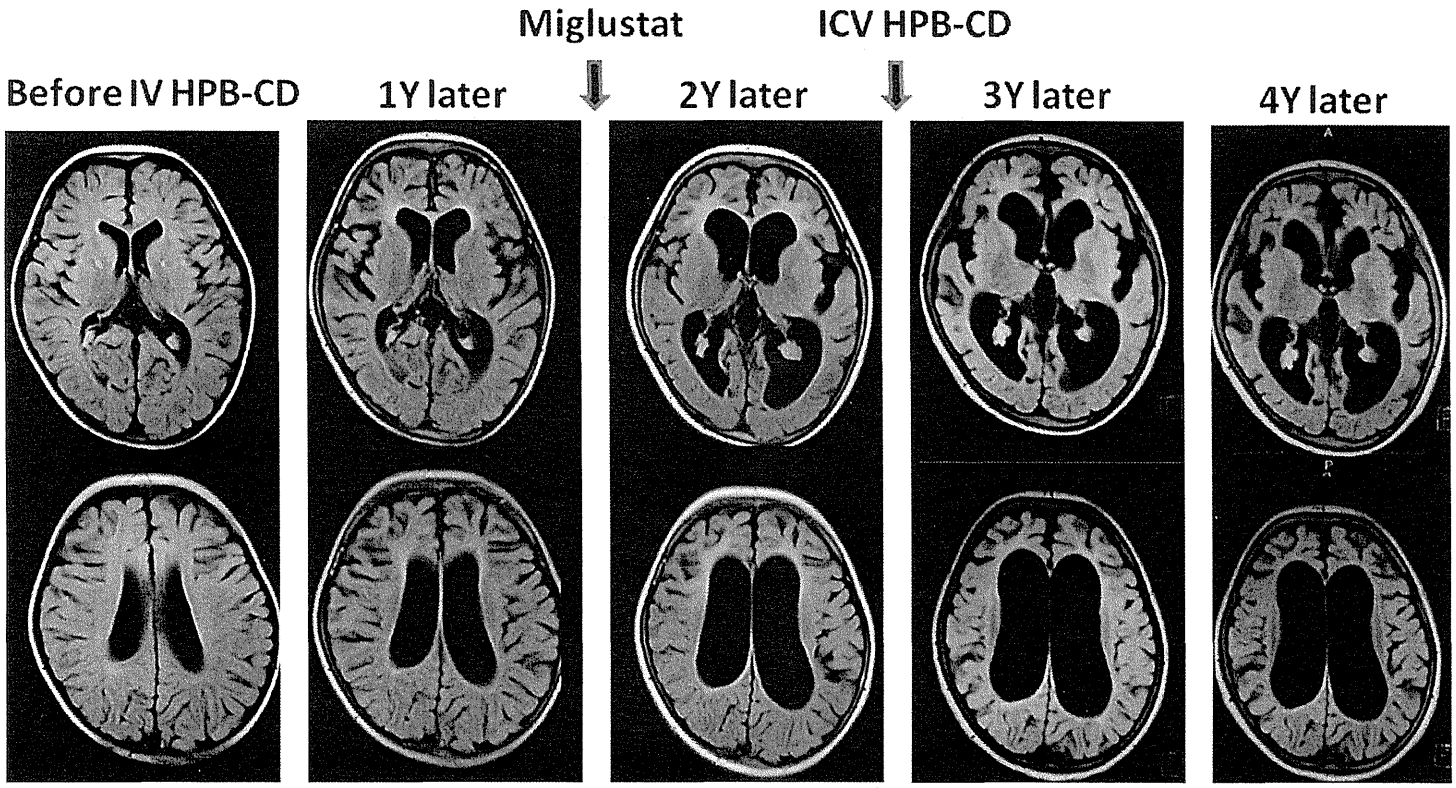

Fig. 2. Changes in MRI (FLAIR, fluid attenuated inversion recovery, images) before and after treatment with 2-hydroxypropyl-β-cyclodextrin. Miglustat was added after 1 year of treatment. Progressive brain atrophy is visible especially before the ICV HPB-CD therapy.

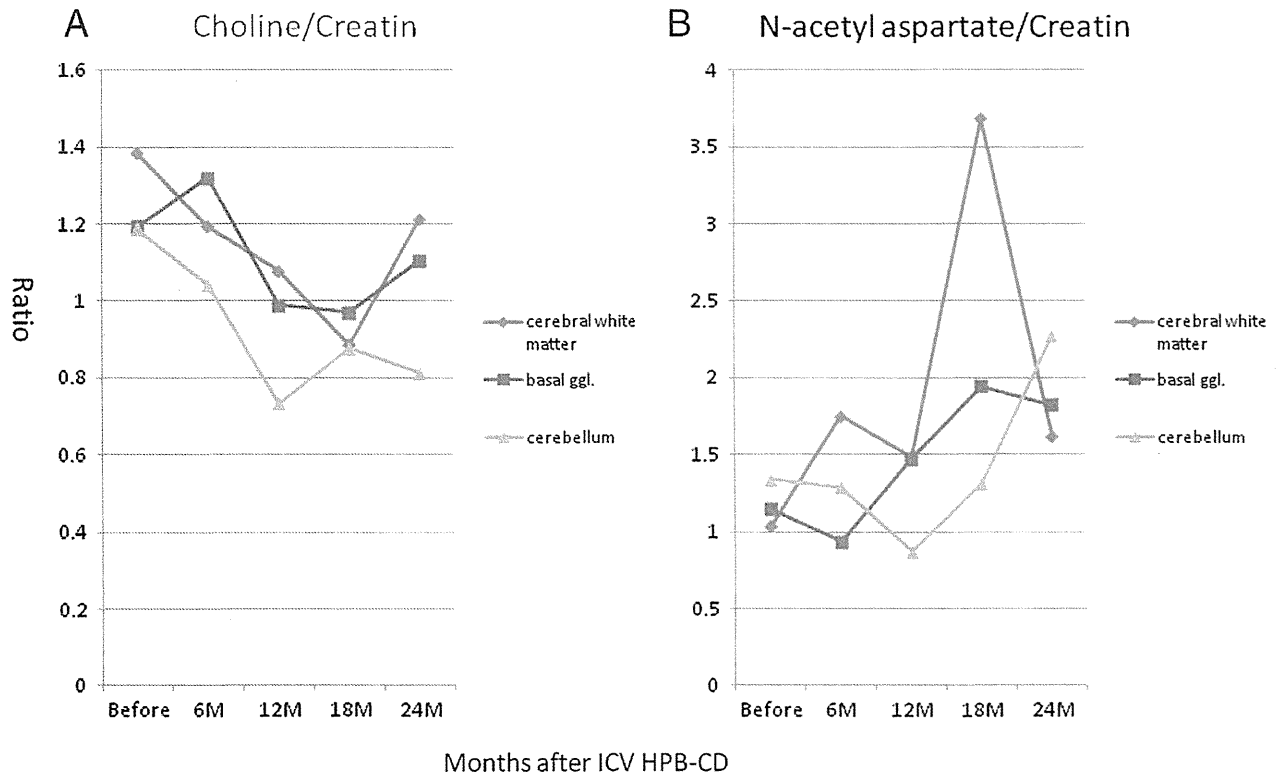

Fig. 3. (A) Changes in the choline to creatine ratio (Cho/Cr) of MRS in the cerebral white matter, basal ganglia, and cerebellum. (B) Changes in the N-acetylaspartate to creatine ratio (NAA/Cr) of MRS in the cerebral white matter, basal ganglia, and cerebellum.

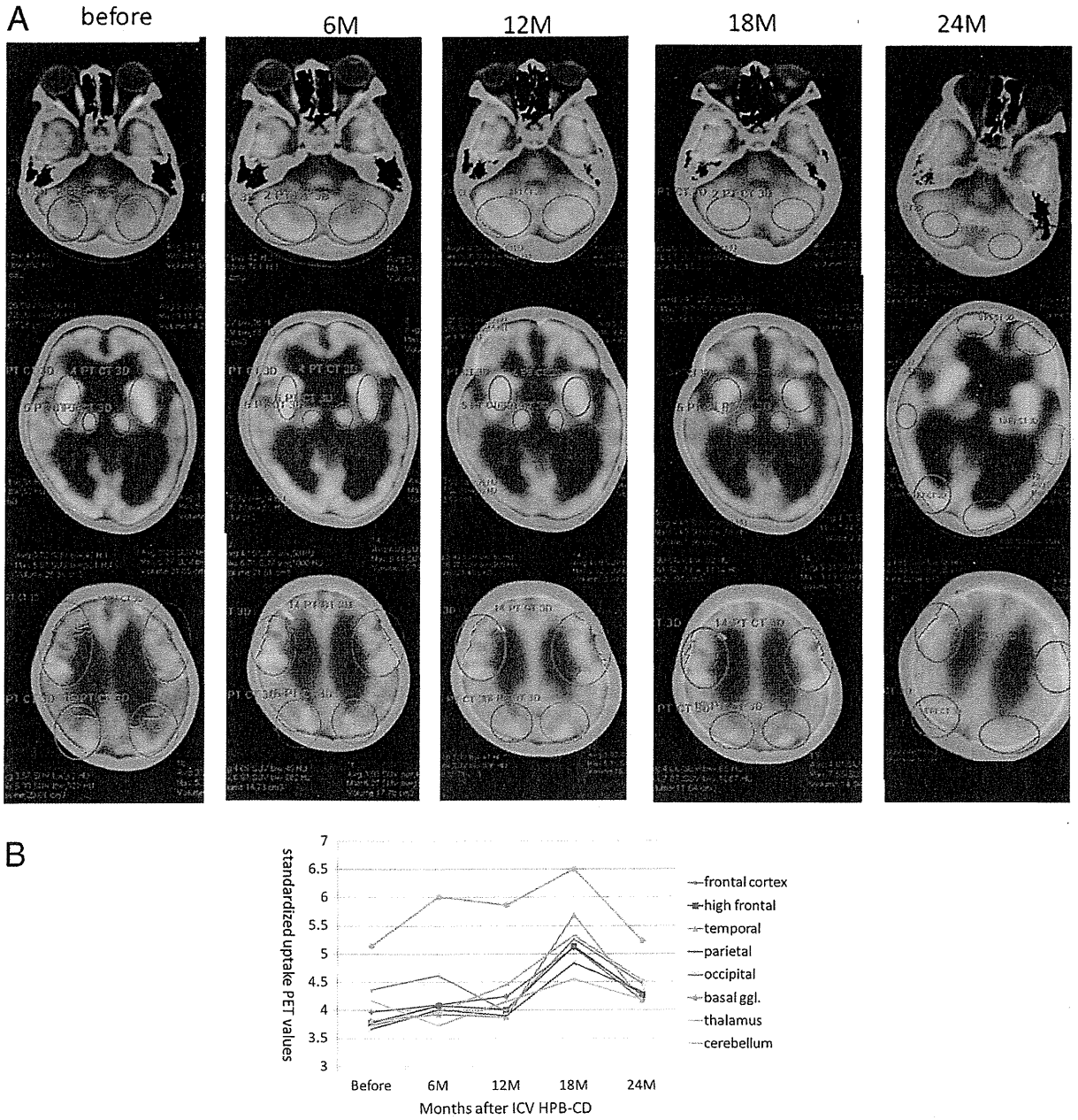

Fig. 4. (A) Changes in PET images after ICV HPB-CD. The cerebral cortex and cerebellum looks brighter than before. (B) Changes in standardized uptake PET values after ICV HPB-CD. The uptake values reached the peak 18 months after ICV HPB-CD in every region.

effects from ABR studies even after two years of treatment with frequent intrathecal administration (Data not shown).

A recent study using sensitive liquid chromatography–tandem mass spectrometry described the concentrations of HPB-CD in CSF and plasma after an intrathecal injection of HPB-CD at a dose of 50 mg in 3 patients with NPC, where the clearance, volume of distribution, and half life were 18–19 mL/h, ~130 mL, and 6.58–10.1 h, respectively [13]. Due to the limited sensitivity of our analytical methods in the present study, the concentrations of HPB-CD in CSF seemed comparable to those with initial distribution phase after the intrathecal injection. During the distribution phase after the ICV injection, the concentrations of HPB-CD in CSF were in the range at which HPB-CD could normalize cellular cholesterol abnormality in vitro [14,15]. In addition, the apparent volumes of distribution of HPB-CD estimated from the distribution phase were slightly larger than the CSF volume in children [16]; the volume of distribution of HPB-CD at steady state should be larger than the apparent volume. This indicates that following the ICV injection,

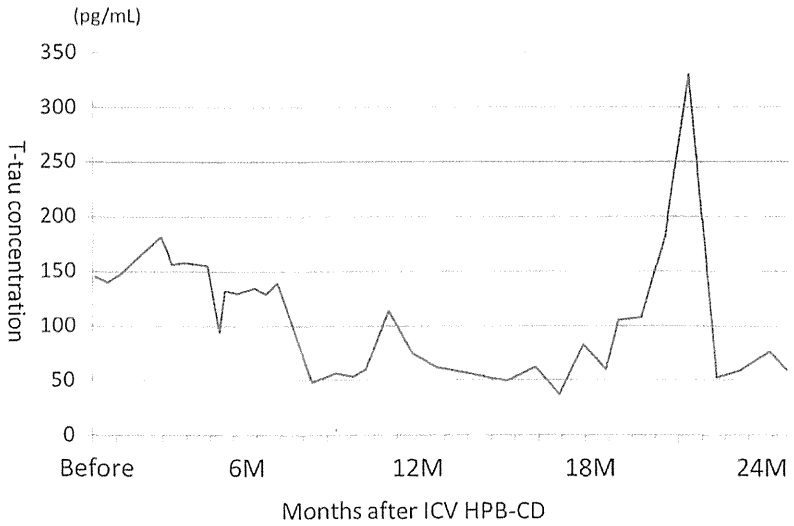

Fig. 5. Changes in CSF T-tau concentration after ICV HPB-CD therapy. The levels of CSF T-tau gradually decreased after the ICV HPB-CD therapy, but were transiently increased from the 21 months to 23 months period, when the dose of HPB-CD reached 300 mg twice a week.

HPB-CD penetrates deeper into the central nervous system beyond the CSF compartment, as suggested by Ottinger et al. in an animal study [8].

The reported ED_{50} in NPC mice is approximately about 0.5 mg/kg, with 35 mg/kg administration of HPB-CD effective for 1 week [4]. An in vitro study using primary cultures of neurons and glial cells from *Npc1*$^{-/-}$ mice also demonstrated that 0.1 mM of HPB-CD is the optimum concentration and that 10 mM is toxic for cells [15]. Our present data combined with these previous observations suggest that 10 mg/kg would be a sufficient dose of ICV HPB-CD, although the optimum intervals for ICV injections of HPB-CD remain unclear. In our experience, the patient looks more alert after several days of HPB-CD injection according to the parents' observation. Thus, we tried twice a week injections of 200 mg HPB-CD. MRS and PET study suggested better results, supported by the observation of slightly lower clearance rates of HPB-CD compared to the CSF turn-over rate of 21–25 mL/h in normal human subjects [13].

In the present study, we showed the efficacy and safety of ICV HPB-CD treatment and the effect on concentrations of HPB-CD in CSF. However, the optimal dose and dosing intervals for ICV HPB-CD remain to be determined, necessitating further studies into the mechanisms of HPB-CD action in NPC.

Supplementary data to this article can be found online at http://dx.doi.org/10.1016/j.ymgmr.2014.08.004.

Acknowledgments

The authors thank Dr. Peter Pentchev for introducing them to Chris Hempel, who generously supplied the protocols for the Hempel twins. The authors also thank Dr. Kaori Adachi and Dr. Eiji Nanba, Tottori University, for the genetic diagnosis of the patient. This work was supported by a JSPS KAKENHI Grant Number 23590642.

References

[1] M.T. Vanier, Niemann–Pick disease type C, Orphanet J. Rare Dis. 5 (2010) 16.
[2] B. Liu, S.D. Turley, D.K. Burns, A.M. Miller, J.J. Repa, J.M. Dietschy, Reversal of defective lysosomal transport in NPC disease ameliorates liver dysfunction and neurodegeneration in the npc1 −/− mouse, Proc. Natl. Acad. Sci. U. S. A. 106 (2009) 2377–2382.
[3] C.D. Davidson, N.F. Ali, M.C. Micsenyi, G. Stephney, S. Renault, K. Dobrenis, D.S. Ory, M.T. Vanier, S.U. Walkley, Chronic cyclodextrin treatment of murine Niemann–Pick C disease ameliorates neuronal cholesterol and glycosphingolipid storage and disease progression, PLoS One 4 (2009) e6951.
[4] A. Aqul, B. Liu, C.M. Ramirez, A.A. Pieper, S.J. Estill, D.K. Burns, J.J. Repa, S.D. Turley, J.M. Dietschy, Unesterified cholesterol accumulation in late endosomes/lysosomes causes neurodegeneration and is prevented by driving cholesterol export from this compartment, J. Neurosci. 31 (2011) 9404–9413.

[5] B. Liu, Therapeutic potential of cyclodextrins in the treatment of Niemann–Pick type C disease, Clin. Lipidol. 7 (2012) 289–301.
[6] T. Irie, K. Uekama, Pharmaceutical applications of cyclodextrins. III. Toxicological issues and safety evaluation, J. Pharm. Sci. 86 (1997) 147–162.
[7] M. Matsuo, K. Togawa, S. Hirabaru, A. Mochinaga, M. Narita, M. Adachi, T. Egashira, T. Irie, K. Ohno, Effects of cyclodextrin in two patients with Niemann–Pick type C disease, Mol. Genet. Metab. 108 (2013) 76–81.
[8] E.A. Ottinger, M.L. Kao, N. Carrillo-Carrasco, N. Yanjanin, R.K. Shankar, M. Janssen, M. Brewster, I. Scott, X. Xu, J. Cradock, P. Terse, S.J. Dehdashti, J. Marugan, W. Zheng, L. Portilla, A. Hubbs, W.J. Pavan, J. Heiss, C.H. Vite, S.U. Walkley, D.S. Ory, S.A. Silber, F.D. Porter, C.P. Austin, J.C. McKew, Collaborative development of 2-hydroxypropyl-β-cyclodextrin for the treatment of Niemann–Pick type C1 disease, Curr. Top. Med. Chem. 14 (2014) 330–339.
[9] H.W. Frijlink, J. Visser, N.R. Hefting, R. Oosting, D.K. Meijer, C.F. Lerk, The pharmacokinetics of beta-cyclodextrin and hydroxypropyl-beta-cyclodextrin in the rat, Pharm. Res. 7 (1990) 1248–1252.
[10] N. Mattsson, H. Zetterberg, S. Bianconi, N.M. Yanjanin, R. Fu, J.E. Månsson, F.D. Porter, K. Blennow, Gamma-secretase-dependent amyloid-beta is increased in Niemann–Pick type C: a cross-sectional study, Neurology 76 (2011) 366–372.
[11] N. Mattsson, H. Zetterberg, S. Bianconi, N.M. Yanjanin, R. Fu, J.E. Månsson, F.D. Porter, K. Blennow, Miglustat treatment may reduce cerebrospinal fluid levels of the axonal degeneration marker tau in Niemann–Pick type C, JIMD Rep. 3 (2012) 45–52.
[12] S. Ward, P. O'Donnell, S. Fernandez, C.H. Vite, 2-hydroxypropyl-beta-cyclodextrin raises hearing threshold in normal cats and in cats with Niemann–Pick type C disease, Pediatr. Res. 68 (2010) 52–56.
[13] H. Jiang, R. Sidhu, H. Fujiwara, M. DeMeulder, R. de Vries, Y. Gong, M. Kao, F.D. Porter, N.M. Yanjanin, N. Carillo—Carasco, X. Xu, E. Ottinger, M. Woolery, D.S. Ory, X. Jiang, Development and validation of sensitive LC—MS/MS assays for quantification of 2-hydroxypropyl-β-cyclodextrin in human plasma and CSF, J. Lipid Res. 55 (2014) 1537–1548.
[14] D. Maetzel, S. Sarkar, H. Wang, L. Abi-Mosleh, P. Xu, A.W. Cheng, Q. Gao, M. Mitalipova, R. Jaenisch, Genetic and chemical correction of cholesterol accumulation and impaired autophagy in hepatic and neural cells derived from Niemann–Pick type C patient-specific iPS cells, Stem Cell Rep. 2 (2014) 866–880.
[15] K.B. Peake, J.E. Vance, Normalization of cholesterol homeostasis by 2-hydroxypropyl-β-cyclodextrin in neurons and glia from Niemann–Pick C1 (NPC1)-deficient mice, J. Biol. Chem. 287 (2012) 9290–9298.
[16] R. Troncin, C. Dadure, Paediatric spinal anaesthesia, Updat. Anaesth. 25 (2009) 22–24.

Biomaterials 45 (2015) 115–123

Contents lists available at ScienceDirect

Biomaterials

journal homepage: www.elsevier.com/locate/biomaterials

Preparation of hydrophilic $C_{60}(OH)_{10}$/2-hydroxypropyl-β-cyclodextrin nanoparticles for the treatment of a liver injury induced by an overdose of acetaminophen

Yoshitaka Umezaki [a, 1], Daisuke Iohara [a, 1], Makoto Anraku [a], Yoichi Ishitsuka [b], Tetsumi Irie [b], Kaneto Uekama [c], Fumitoshi Hirayama [a, *]

[a] Faculty of Pharmaceutical Sciences, Sojo University, 4-22-1 Ikeda, Nishi-ku, Kumamoto 860-0082, Japan
[b] Graduate School of Pharmaceutical Sciences, Kumamoto University, 5-1 Oe-honmachi, Chuo-ku, Kumamoto 862-0973, Japan
[c] DDS Research Institute, Sojo University, 4-22-1 Ikeda, Nishi-ku, Kumamoto 860-0082, Japan

ARTICLE INFO

Article history:
Received 22 September 2014
Accepted 20 December 2014
Available online 20 January 2015

Keywords:
Polyhydroxylated fullerene
Cyclodextrin
Nanoparticle
Antioxidant
Liver
Acetaminophen

ABSTRACT

Stable hydrophilic $C_{60}(OH)_{10}$ nanoparticles were prepared from 2-hydroxypropyl-β-cyclodextrin (HP-β-CD) and applied to the treatment of an acetaminophen overdose induced liver Injury. $C_{60}(OH)_{10}$ nanoparticles were produced by cogrinding α-CD, β-CD, γ-CD and HP-β-CD and characterized in terms of solubility, mean particle diameter, ζ-potential and long term dispersibility in water. Hydrophilic $C_{60}(OH)_{10}$ nanoparticles with particle sizes less than 50 nm were effectively produced by cogrinding HP-β-CD with $C_{60}(OH)_{10}$ at a molar ratio of 1:3 ($C_{60}(OH)_{10}$:CD). The resulting $C_{60}(OH)_{10}$/HP-β-CD nanoparticles were stable in water and showed no aggregation over a 1 month period. The $C_{60}(OH)_{10}$/CDs nanoparticles scavenged not only free radicals (DPPH and ABTS radicals) but also reactive oxygen species ($O_2^{\bullet-}$ and •OH). When $C_{60}(OH)_{10}$/HP-β-CD nanoparticles were intraperitoneally administered to mice with a liver injury induced by an overdose of acetaminophen (APAP), the ALT and AST levels were markedly reduced to almost the same level as that for normal mice. Furthermore, the administration of the nanoparticles prolonged the survival rate of liver injured mice, while all of the mice that were treated with APAP died within 40 h. To reveal the mechanism responsible for liver protection by $C_{60}(OH)_{10}$ nanoparticles, GSH level, CYP2E1 expression and peroxynitrite formation in the liver were assessed. $C_{60}(OH)_{10}$/HP-β-CD nanoparticles had no effect on CYP2E1 expression and GSH depletion, but suppressed the generation of peroxynitrite in the liver. The findings indicate that the protective effect of $C_{60}(OH)_{10}$/HP-β-CD nanoparticles was due to the suppression of oxidative stress in mitochondria, as the result of scavenging ROS such as $O_2^{\bullet-}$, NO and peroxynitrite, which act as critical mediators in the liver injuries.

1. Introduction

Fullerenes, large spherical molecules composed of only carbon atoms, have been of great interest for practical applications that exploit their unique electronic properties and biological activities [1]. The fullerene family, especially C_{60}, has appealing photo-, electro-chemical and physical properties, which have been exploited in various medical fields [2]. For example, it can function as a radical scavenger [3], an antioxidant [4] and as a gene carrier [5] or in drug delivery [6]. However, these potential biomedical applications of C_{60} have been hampered by its extremely poor solubility in water [7,8], thus various fullerene derivatives have been synthesized in attempts to overcome the drawback associated with the limited solubility of C_{60}. Polyhydroxylated fullerenes (fullerenol, $C_{60}(OH)_n$), some of the simplest C_{60} derivatives, show improved solubility in aqueous media. The number of hydroxyl groups introduced into a C_{60} molecule is a key factor for enhancing the hydrophilicity of the material as well as its biological activity [9,10]. Fullerenols are regarded as potential candidates for use in scavenging reactive oxygen species (ROS), which arise due to neuroprotective [11] and cytoprotective [12] effects by reducing oxidative stress. It has been reported that $C_{60}(OH)_{24}$ directly quenches nitric oxide (NO) and blocks its biological activity *in vivo* [13]. Injac et al. reported that

* Corresponding author. Tel.: +81 96 326 4098; fax: +81 96 326 5048.
E-mail address: fhira@ph.sojo-u.ac.jp (F. Hirayama).
[1] These authors equally contributed to the work.

http://dx.doi.org/10.1016/j.biomaterials.2014.12.032
0142-9612/

$C_{60}(OH)_{24}$ exerts an organo-protective effect on the cardiotoxicity induced by doxorubicin [14]. However, these studies were conducted using water as a solvent or biological media including dimethyl sulfoxide, in which fullerenols were suspended or were present in the form of large aggregates. Although fullerenols are more soluble than unmodified C_{60}, further enhancement in their solubility is necessary for a precise evaluation of their biological activities and for extensive biomedical applications. In addition, some researchers have reported that fullerenol shows cytotoxic effects that are dependent on the number of hydroxyl groups contained by the molecule [15,16]. Therefore using fullerenol with a minimum number of hydroxyl groups would be a desirable approach for pharmaceutical applications of fullerenol.

Acetaminophen (paracetamol, *N*-acetyl-*p*-aminophenol (APAP)) is a widely used analgesic and antipyretic drug. While there are generally few side effects when the recommended dose is used, an overdose causes hepatic injury and is the most frequent cause of the acute liver failure in the United State, the United Kingdom and other countries [17–19]. The development and progression of liver injury induced by APAP is related to the production of ROS [20], such as superoxide anions and peroxynitrite [21,22], the release of cytokines [23] and eicosanoids [24]. *N*-acetylcysteine (NAC) is used to treat patients with an APAP overdose. However, the efficacy is limited and a novel approach for addressing this issue is required.

In a previous study, we reported on the preparation of stable C_{60} nanoparticles (mean particle size ca. 90 nm), the surfaces of which were covered by a hydrophilic 2-hydroxypropyl-β-cyclodextrin (HP-β-CD) through physical adsorption and weak hydrophobic interactions [25]. The C_{60} nanoparticles maintained their small particle size in water for periods of over 1 month and no evidence of aggregation was found. In this study, we report on the preparation of stable hydrophilic $C_{60}(OH)_{10}$ nanoparticles using HP-β-CD and an evaluation of its biological activities was conducted, with respect to issues such as the free radicals and ROS scavenging ability. Furthermore, a protective effect against APAP overdose induced liver injury was studied with comparing the effect of NAC.

2. Materials and methods

2.1. Materials

$C_{60}(OH)_{10}$ (nanom spectra D100) was purchased from Frontier Carbon Co. (Tokyo, Japan) and was confirmed by mass spectrometry that approximately 10 hydroxyl groups were introduced in a molecule. 2-Hydroxypropyl-β-CD (HP-β-CD, the degree of substitution (D.S.) of the 2-hydroxypropyl group was 5.6) and parent CDs (α-CD, β-CD and γ-CD) were gifts from Nihon Shokuhin Kako Co., Ltd. (Tokyo, Japan). APAP and NAC were purchased from Wako Pure Chemical Industries, Ltd. (Tokyo, Japan). The 1,1′-diphenyl-2-picrylhydrazyl (DPPH) and 2,2′-azinobis(3-ethylbenzothiazoline-6-sulfonic acid) (ABTS) reagents were supplied by Nacalai Tesque (Kyoto, Japan). 5,5-Dimethy-1-pyrroline *N*-oxide (DMPO) was purchased from Labotec Co. Ltd. (Tokyo, Japan). Sodium nitroprusside dehydrate (SNP) was purchased from Sigma–Aldrich Co. LLC (Tokyo, Japan). Dihydrorhodamine 123 was purchased from Cayman Chemical Company (Michigan, USA). Peroxynitrite solution was purchased from Chemical Dojin Co. Ltd. (Kumamoto, Japan). All other materials and solvents were of analytical reagent grade and Milli-Q water was used throughout the study.

2.2. Preparation and characterization of $C_{60}(OH)_{10}$/HP-β-CD nanoparticles

$C_{60}(OH)_{10}$ (15 mg) was ground with α-CD (49 mg), β-CD (57 mg), γ-CD (66 mg) or HP-β-CD (73 mg) in different molar ratios (generally 1:3 for guest:host), using an automatic magnetic agitating mortar (MNV-01, AS ONE, Tokyo, Japan) for 3 h at 4 °C under reduced pressure [25]. The pulverized C_{60}/CDs material was dispersed in water by ultrasonication for 5 min, to give approximately 1 mM of $C_{60}(OH)_{10}$. The resulting solutions were syringe-filtered through a 0.2 μm pore size filter. Particle sizes of the $C_{60}(OH)_{10}$/CDs nanoparticles were determined by dynamic light scattering (DLS-8000HL, Otsuka Electronics Co., Ltd. Tokyo, Japan) equipped with a He–Ne laser (10 mW) operating at 632.8 nm. DLS measurements were performed at a scattering angle of 90°. The autocorrelation function was analyzed by the cumulant method to obtain the average particle diameter. Zeta potentials for the colloids were determined by a Zetasizer (Nano-zs, Sysmex Co., Tokyo, Japan). Transmission electron microscopy (TEM) images were obtained on a JEM-1400Plus (JEOL, Tokyo, Japan) operating at 100 kV. Specimens for TEM observations were prepared by immersing a 150 mesh copper grid coated with a carbon film in the sample solution ($C_{60}(OH)_{10}$ = 0.05 μM) including uranyl acetate to stain the sample.

2.3. Free radical scavenging activity of $C_{60}(OH)_{10}$/HP-β-CD nanoparticles

The radical scavenging ability of $C_{60}(OH)_{10}$ nanoparticles was studied using DPPH and ABTS radicals. Different concentrations of $C_{60}(OH)_{10}$ nanoparticles (5–250 μM) were tested in 50% ethanolic solutions of DPPH (0.2 mM). Radical scavenging ability was estimated from the decrease in absorbance of the DPPH radical at 540 nm [26] due to the reaction with $C_{60}(OH)_{10}$, using Eq. (1) below.

Radical scavenging activity (%) = 100− (absorbance with samples/absorbance without samples) × 100. (1)

Stable ABTS cation radicals were generated by oxidation with potassium persulfate. The reaction mixture contained 2.45 mM potassium persulfate and 2 mM ABTS in distilled water and, after 1 day, the resulting stable ABTS radical was used in the assay. The ABTS solutions were diluted by 10% with PBS, and then mixed with sample solutions at a ratio of 9:1. The reaction of $C_{60}(OH)_{10}$ with ABTS radicals was monitored based on the decrease in its absorbance at 734 nm [27], using Eq. (1).

2.4. ROS scavenging activity of $C_{60}(OH)_{10}$/CD nanoparticles

To evaluate the ROS scavenging ability of $C_{60}(OH)_{10}$/CDs nanoparticles, $O_2^{\bullet-}$ was enzymatically generated by treating hypoxanthine with xanthine oxidase and •OH was generated via the Fenton reaction [28]. The generation of $O_2^{\bullet-}$ was measured by means of an X-band electron spin resonance (ESR) spectrometer (JES-FA100, JEOL Ltd., Tokyo, Japan) under the following conditions: microwave frequency 9.417 GHz, microwave power 4 mW, field modulation 0.1 mT at 100 kHz and sweep time 30s. $O_2^{\bullet-}$ was detected using DMPO as a spin-trapping reagent. One hundred microliter aliquots of sample solutions, 60 μL of 0.67 mM hypoxanthine, 20 μL of 0.8 unit/mL of xanthine oxidase and 20 μL of DMPO were vigorously mixed well under aerobic conditions. The mixed solutions were collected in a flat cell, then immediately subjected to ESR measurement. •OH was also detected by ESR using DMPO as a spin-trapping reagent. One hundred microliters of a sample solution, 40 μL of 4.4 mM H_2O_2, 40 μL of 1 μM $FeSO_4$ solution and 20 μL of DMPO were well mixed under aerobic conditions and subjected to ESR measurements. Scavenging ability of $C_{60}(OH)_{10}$ to $O_2^{\bullet-}$ and •OH species was evaluated by the reduction in ESR intensities of DMPO-OOH and DMPO-OH adducts, respectively, compared to the intensities observed in the absence of $C_{60}(OH)_{10}$, using Eq. (2).

ROS scavenging activity (%) = 100− (relative intensity with samples/relative intensity without samples) x 100. (2)

2.5. Protective effect of $C_{60}(OH)_{10}$/HP-β-CD nanoparticles on APAP overdose induced liver injury mice

An APAP overdose induced liver injury model was prepared according to the method reported by Ishituka et al. [29]. Male 7-9 week-old C57BL6 mice (Japan SLC, Inc., Shizuoka, Japan) were fasted overnight, but had free access to water prior to the experiments. APAP was dissolved in PBS and administered to the mice intraperitoneally (400 mg/kg). At 30 min after the APAP injection, $C_{60}(OH)_{10}$/HP-β-CD nanoparticles ($C_{60}(OH)_{10}$ = 100 or 200 mg/kg) or NAC (200 mg/kg) were administered intraperitoneally. The mice were sacrificed at 24 h after APAP injection, and blood and liver samples were collected. Blood samples were centrifuged at 4000 × g at 4 °C for 10 min, and serum ALT and AST levels were measured. The care and maintenance of animals was in accordance with the institutional guidelines of the Institutional Animal Care and Use Committee of Sojo University.

2.6. CYP2E1 expression

The expression of the CYP2E1 protein in the liver was determined by western blotting. Protein samples were subjected to SDS-PAGE on a 10% polyacrylamide gel. Proteins were electroblotted onto a PVDF membrane (Millipore Corp., Bedford, MA, USA). After blocking with 5% skim milk, the membranes were washed three times and treated with the primary antibody. Primary antibodies were diluted in 5% skim milk at the following dilutions: anti-CYP2E1 antibodies (Abcam, Inc., Cambridge, MA, USA) (1:2500) or anti-β-actin (Cell Signaling Technology, Danvers, MA, USA) (1:1000), incubated overnight at 4 °C. The membranes were washed three times with TBS in Tween-20 and then incubated with HRP-conjugated secondary antibodies (Cell Signaling Technology). The blots were visualized using SuperSignal (Pierce, Rockford, IL, USA) and measured by ImageQuant LAS 4000mini (GE Healthcare Japan, Tokyo, Japan).

2.7. Hepatic total glutathione contents

The liver tissue samples were weighed and stored at −80 °C until used in assays. Tissue homogenates were prepared in 5% metraphosphoric acid solution at a 1:5 (w/v) ratio and centrifuged for 10 min at 1000 g at 4 °C. The supernatant was collected

and total GSH concentration was measured by a BIOXYTECH GSH/GSSG-412 (OXIS Health Products, Inc, Portland, OR, USA) according to the manufacturer's protocol.

2.8. Immunohistochemistry (anti-nitrotyrosine)

To evaluate nitrotyrosine formation, an immunohistochemical analysis using an anti-nitrotyrosine polyclonal antibody (Merck Millipore) was performed. The microtome sections were incubated overnight at 4 °C with an anti-nitrotyrosine antibody (1:500 dilution) and then stained with Histofine® Simple Stain MAX PO (Nichirei Biosciences, Tokyo, Japan). Following the washing step, 3,3-diaminobenzidine was applied to the sections, which were then incubated with Mayer's hematoxylin. The liver histopathological changes were visualized and analyzed using a microscope system (BIOREVO BZ-9000; Keyence Co., Osaka, Japan).

2.9. Nitric oxide (NO) and peroxynitrite scavenging activity of $C_{60}(OH)_{10}$/HP-β-CD nanoparticles

To estimate the NO scavenging activity of $C_{60}(OH)_{10}$/HP-β-CD nanoparticles, sodium nitroprusside (SNP) was used as a potent NO donor [13]. 40 μL of 1 mM SNP solution was mixed with 40 μL of $C_{60}(OH)_{10}$/HP-β-CD nanoparticles at various concentrations in a 96 well plate. The plate was irradiated for 5 min at 35 mW/cm^2 from a xenon light source (MAX-303, Asahi spectra Co., Ltd., Tokyo, Japan) to produce a constant level of NO. The resulting NO was detected by means of a Griess reagent kit (Chemical Dojin Co. Ltd, Kumamoto, Japan) and measured UV at 540 nm. Peroxynitrite was evaluated by the oxidation of dihydrorhodamine 123. 50 μL of gelatin (1.2 mg/mL), 50 μL of dihydrorhodamine 123 (0.1 mM) and 50 μL of $C_{60}(OH)_{10}$/HP-β-CD were added to a 96 well plate, and then incubated for 5 min. A fifty microliter aliquot of the peroxynitrite solution (0.28 mM) was added to the above prepared solution. After a 5 min incubation, the fluorescence was measured at 535 nm for rhodamine emission.

3. Results

3.1. Preparation and characterization of $C_{60}(OH)_{10}$/CD nanoparticles

$C_{60}(OH)_{10}$ was ground with α-CD, β-CD, γ-CD and HP-β-CD at various molar ratios using the magnetic agitating mortar described in the experimental section. The resulting powders were dispersed in water and the resulting suspensions were passed through a 0.2 μm pore size filter. As shown in Fig. 1, the filtrate of the $C_{60}(OH)_{10}$ solutions prepared with HP-β-CD or γ-CD was a transparent dark red-colored solution, indicating that $C_{60}(OH)_{10}$ was completely dissolved in the solution. Light yellow-colored solutions were obtained in the case of the $C_{60}(OH)_{10}$/α-CD and/β-CD systems. On the other hand, transparent solutions with no color were obtained for a ground sample of $C_{60}(OH)_{10}$ alone, because it was largely present in the form of large aggregated states in the absence of CDs and thus $C_{60}(OH)_{10}$ particles were completely removed by the 0.2 μm filter. The effect of CDs on the solubility of $C_{60}(OH)_{10}$ in water is shown in Fig. 1. The $C_{60}(OH)_{10}$ concentration in the filtrate increased with increasing amount of CD added to the grinding mixture, whereas $C_{60}(OH)_{10}$ was not detected in the filtrate for the $C_{60}(OH)_{10}$ sample ground without CDs. HP-β-CD and γ-CD produced high $C_{60}(OH)_{10}$ concentrations, i.e. about 750 μM at a molar ratio of 1:3 ($C_{60}(OH)_{10}$: CD). Highly water soluble HP-β-CyD and γ-CD can pass through a 0.2 μm filter without being adsorbed to the filter, thus the actual molar ratio of $C_{60}(OH)_{10}$: CD in the filtrate was 1:4, when the $C_{60}(OH)_{10}$/CD (1:3) powder was dispersed in water. In the case of α-CD and β-CD, the $C_{60}(OH)_{10}$ concentration was lower compared to the others. The particle size and ζ-potential of

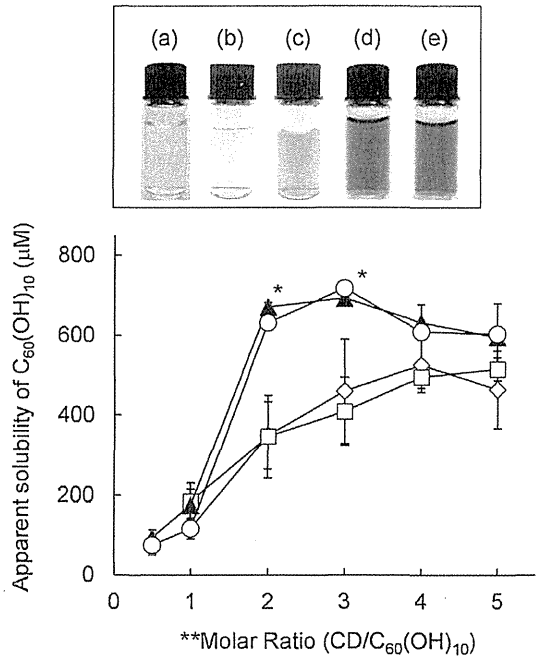

Fig. 1. Apparent solubility of $C_{60}(OH)_{10}$/CDs ground mixtures prepared at various molar ratios and the appearances of filtrates after filtration through a 0.2 μm Filter. Each point represents the mean ± S.E. of 3–4 experiments. *, $p < 0.05$ *versus* $C_{60}(OH)_{10}$/α-CD and/β-CD. **Molar ratio of CDs/$C_{60}(OH)_{10}$ during grinding process. ◇: $C_{60}(OH)_{10}$/α-CD, □: $C_{60}(OH)_{10}$/β-CD, ▲: $C_{60}(OH)_{10}$/γ-CD, ○: $C_{60}(OH)_{10}$/HP-β-CD. (a) $C_{60}(OH)_{10}$ alone, (b) $C_{60}(OH)_{10}$/α-CD, (c) $C_{60}(OH)_{10}$/β-CD, (d) $C_{60}(OH)_{10}$/γ-CD, (e) $C_{60}(OH)_{10}$/HP-β-CD.

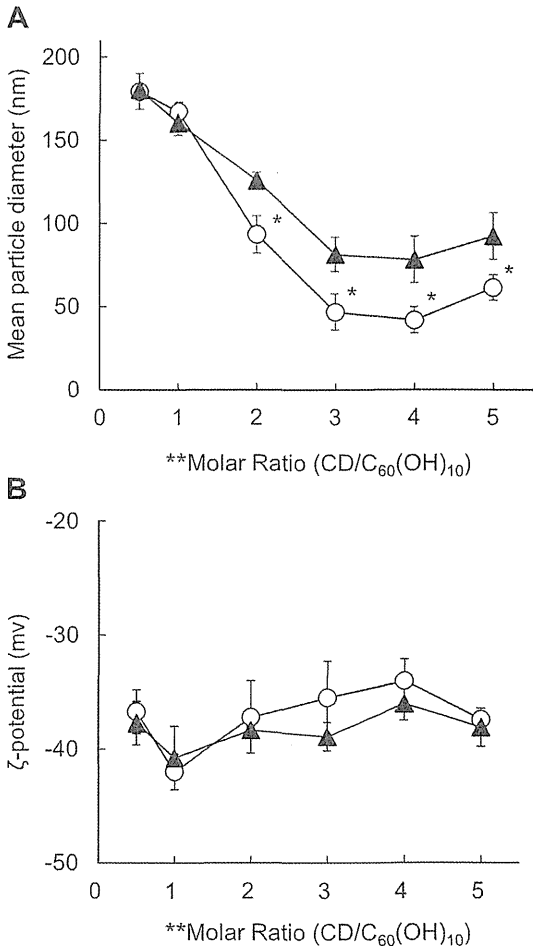

Fig. 2. Particle size (A) and ζ-potential (B) of $C_{60}(OH)_{10}$/HP-β-CD and/γ-CD nanoparticles prepared using various amounts of CDs. Each point represents the mean ± S.E. of 3 experiments. *, $p < 0.05$ *versus* $C_{60}(OH)_{10}$/γ-CD. **Molar ratio of CDs/$C_{60}(OH)_{10}$ during grinding process. ○: $C_{60}(OH)_{10}$/HP-β-CD, ▲: $C_{60}(OH)_{10}$/γ-CD.

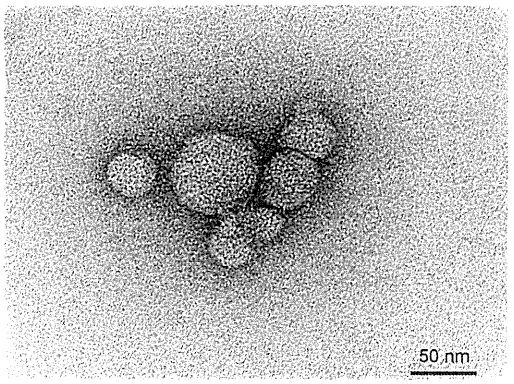

Fig. 3. TEM images of $C_{60}(OH)_{10}$/HP-β-CD nanoparticles.

$C_{60}(OH)_{10}$ nanoparticles found for HP-β-CD and γ-CD are shown in Fig. 2. The mean diameter of the particles decreased with increasing CD/$C_{60}(OH)_{10}$ molar ratio, and became constant for a molar ratio of 1:3 ($C_{60}(OH)_{10}$: CD), reaching less than 50 and 80 nm diameters for the HP-β-CD and γ-CD systems, respectively. The presence of HP-β-CD significantly reduced the particle size of $C_{60}(OH)_{10}$ compared to γ-CD. The ζ-potential of the $C_{60}(OH)_{10}$ nanoparticles was also decreased to negative values by the addition of HP-β-CD and γ-CD, reaching −41 mv at a molar ratio of 1:1 ($C_{60}(OH)_{10}$:CD). No differences in the ζ-values were found between the HP-β-CD and γ-CD systems. This large negative value may contribute to the high dispersibility of the $C_{60}(OH)_{10}$ nanoparticles in water. The morphology of $C_{60}(OH)_{10}$/HP-β-CyD nanoparticles in the water was determined by TEM observations (Fig. 3). The resulting images revealed that $C_{60}(OH)_{10}$/HP-β-CyD nanoparticles were comprised of fairly uniform spheres with a mean diameter of 50 nm. $C_{60}(OH)_{10}$ nanoparticles that were prepared at a molar ratio of 1:3 ($C_{60}(OH)_{10}$: CD) were stored in the dark at 25 °C to evaluate long term stability. As shown in Fig. 4, $C_{60}(OH)_{10}$/HP-β-CD and/γ-CD nanoparticles were stable in water, with the initial diameters (50 nm and 80 nm, respectively) maintained constant for over 1 month, and no aggregation was observed during storage. These collective results indicate that HP-β-CD and γ-CD are useful for solubilizing $C_{60}(OH)_{10}$ as hydrophilic nanoparticles in water. Therefore, the following studies were conducted focusing on $C_{60}(OH)_{10}$/HP-β-CD and $C_{60}(OH)_{10}$/γ-CD nanoparticles prepared at a molar ratio of 1:3 ($C_{60}(OH)_{10}$:CD).

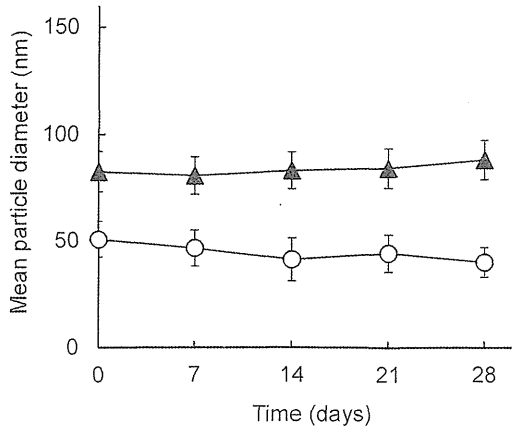

Fig. 4. Dispersibility of $C_{60}(OH)_{10}$/HP-β-CD and/γ-CD nanoparticles in water at 25 °C for long period. Each point represents the mean ± S.E. of 3 experiments. ○: $C_{60}(OH)_{10}$/HP-β-CD, ▲: $C_{60}(OH)_{10}$/γ-CD.

3.2. Evaluation of antioxidant ability of $C_{60}(OH)_{10}$/HP-β-CD and/γ-CD nanoparticles

The antioxidant ability of $C_{60}(OH)_{10}$/CDs nanoparticles was evaluated based on their scavenging effect on the stable free radicals (DPPH and ABTS radicals) and ROS ($O_2^{\bullet-}$ and •OH), in comparison with that of a $C_{60}(OH)_{10}$ suspension prepared by the sonication of $C_{60}(OH)_{10}$ alone in water for 1 h. Fig. 5A shows the scavenging effect of $C_{60}(OH)_{10}$/HP-β-CD and/γ-CD nanoparticles on DPPH radicals. Both $C_{60}(OH)_{10}$/CD nanoparticles scavenged DPPH radicals in a concentration dependent manner. The HP-β-CD nanoparticles showed a tendency to scavenge DPPH radical more effectively than the γ-CD nanoparticles at high $C_{60}(OH)_{10}$ concentrations, although the difference was not significant. On the other hand, the scavenging effect of $C_{60}(OH)_{10}$ alone on DPPH radicals was low, as expected. The scavenging ability of $C_{60}(OH)_{10}$ nanoparticles for ABTS radicals is shown in Fig. 5B. $C_{60}(OH)_{10}$/HP-β-CD

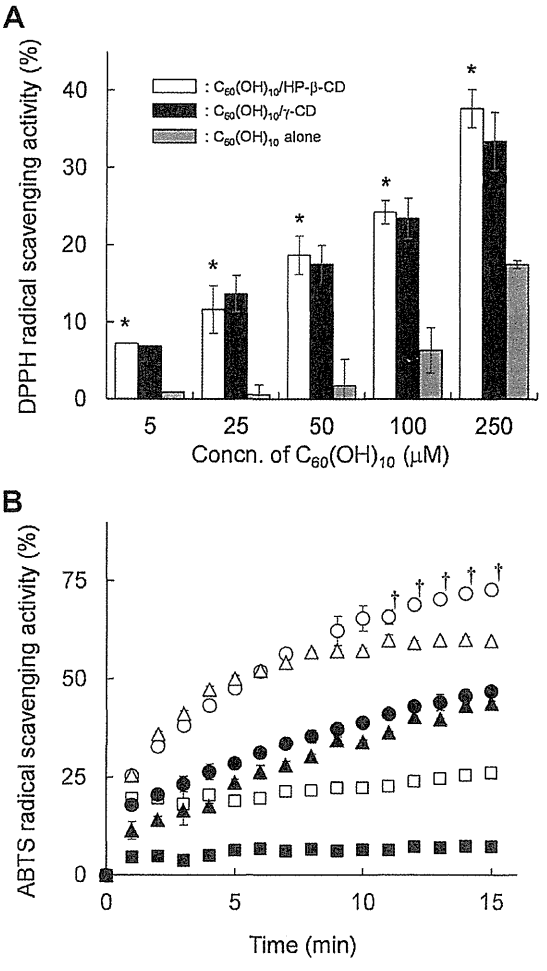

Fig. 5. DPPH radical (A) and ABTS radical (B) scavenging activity of $C_{60}(OH)_{10}$/HP-β-CD nanoparticles and/γ-CD nanoparticles. Each value represents the mean ± S.E. of 3 experiments. *, $p < 0.05$ *versus* $C_{60}(OH)_{10}$ alone. †, $p < 0.05$ *versus* $C_{60}(OH)_{10}$/γ-CD Nanoparticles. ○: $C_{60}(OH)_{10}$/HP-β-CD ($C_{60}(OH)_{10}$ = 200 μM), ●: $C_{60}(OH)_{10}$/HP-β-CD ($C_{60}(OH)_{10}$ = 100 μM), △: $C_{60}(OH)_{10}$/γ-CD ($C_{60}(OH)_{10}$ = 200 μM), ▲: $C_{60}(OH)_{10}$/γ-CD ($C_{60}(OH)_{10}$ = 100 μM), □: $C_{60}(OH)_{10}$ alone ($C_{60}(OH)_{10}$ = 200 μM), ■: $C_{60}(OH)_{10}$ alone ($C_{60}(OH)_{10}$ = 100 μM).

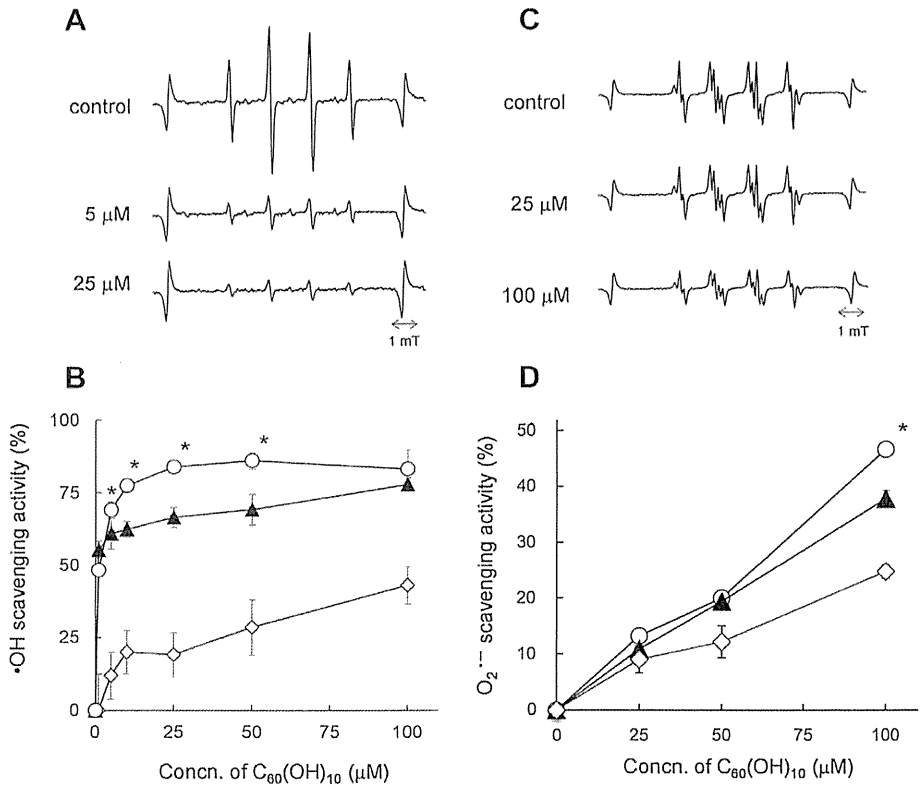

Fig. 6. ESR spectra of DMPO-OH (A) and DMPO-OOH (C) adducts in the presence and absence of $C_{60}(OH)_{10}$/HP-β-CD and •OH (B) and $O_2^{\bullet-}$ (D) scavenging ability of $C_{60}(OH)_{10}$/HP-β-CD and/γ-CD nanoparticles. Each point represents the mean ± S.E. of 3 experiments. *, $p < 0.05$ *versus* $C_{60}(OH)_{10}$/γ-CD. ○: $C_{60}(OH)_{10}$/HP-β-CD, ▲: $C_{60}(OH)_{10}$/γ-CD, ◇: $C_{60}(OH)_{10}$ alone.

nanoparticles reduced ABTS radicals in the same manner as observed for DPPH radicals. The scavenging ability approached 75% for $C_{60}(OH)_{10}$/HP-β-CD nanoparticles at 200 μM of $C_{60}(OH)_{10}$, while that of $C_{60}(OH)_{10}$/γ-CD nanoparticles was 60% at the same concentration. The $C_{60}(OH)_{10}$ alone had less scavenging ability for ABTS radicals.

ROS such as $O_2^{\bullet-}$ and •OH lead to cell death and trigger various diseases related to oxidative stress. Therefore, the scavenging effect of $C_{60}(OH)_{10}$/CD nanoparticles on $O_2^{\bullet-}$ and •OH species was evaluated by means of an ESR spin-trapping method, by monitoring the intensity of ESR signals of DMPO-OH and DMPO-OOH adducts produced by the reaction of DMPO with •OH and $O_2^{\bullet-}$ species, respectively. The ESR intensities of the DMPO-OH adduct (Fig. 6A) and the DMPO-OOH adduct (Fig. 6C) were reduced by the addition of $C_{60}(OH)_{10}$/HP-β-CD nanoparticles, indicating that •OH and $O_2^{\bullet-}$ species were scavenged. The relative intensity of the DMPO-OH and DMPO-OOH adducts compared to an external reference of Mn^{2+} was plotted to calculate the scavenging ability

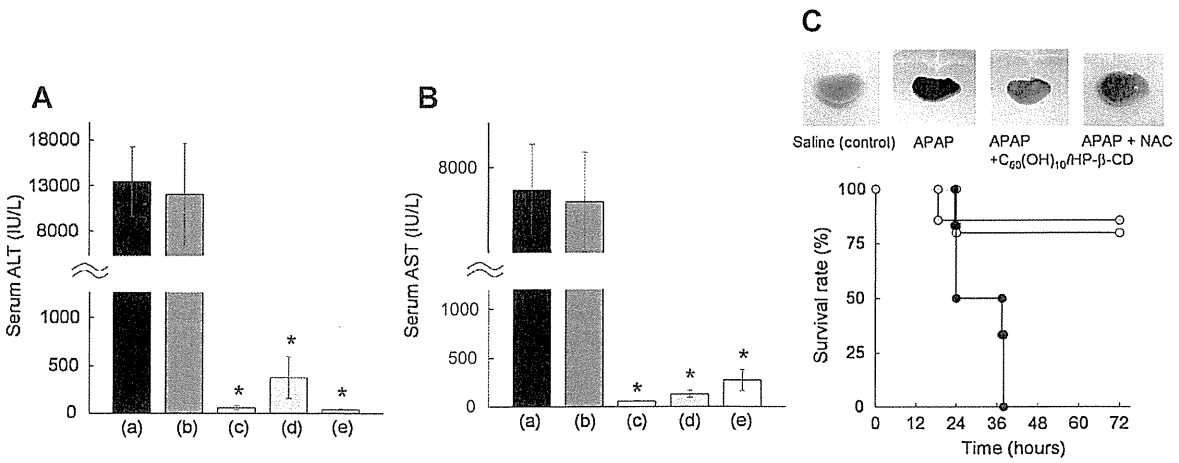

Fig. 7. Effect of $C_{60}(OH)_{10}$/HP-β-CD nanoparticles on ALT (A), AST (B) levels and survival rate (C) in APAP induced liver injury mice. Each value represents the mean ± S.E. of 4–5 experiments. *, $p < 0.05$ *versus* APAP alone. (a) no treatment, (b) $C_{60}(OH)_{10}$ alone suspension, (c) $C_{60}(OH)_{10}$/HP-β-CD 100 mg/kg, (d) $C_{60}(OH)_{10}$/HP-β-CD 200 mg/kg, (e) NAC 200 mg/kg. ●: APAP, ○: APAP + $C_{60}(OH)_{10}$/HP-β-CD, ◎: APAP + NAC.

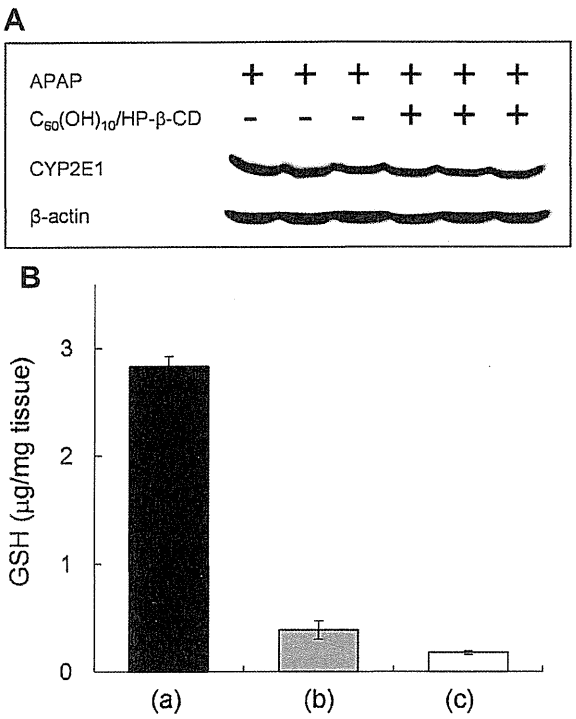

Fig. 8. Effect of $C_{60}(OH)_{10}$/HP-β-CD nanoparticles on CYP2E1 expression (A) and GSH depletion (B) in the liver. (a) normal mice (control), (b) administration of APAP (400 mg/kg), (c) administration of APAP (400 mg/kg) + $C_{60}(OH)_{10}$/HP-β-CD (200 mg/kg).

(%) of the $C_{60}(OH)_{10}$ nanoparticles. As shown in Fig. 6B and D, $C_{60}(OH)_{10}$ nanoparticles scavenged these ROS, especially •OH, by 50% even at 5 μM of $C_{60}(OH)_{10}$. The scavenging ability of the HP-β-CD nanoparticles was larger than that of the γ-CD nanoparticles. The ROS scavenging ability of the $C_{60}(OH)_{10}$ alone suspension was low, similar to the results of the free radical scavenging studies using DPPH and ABTS radicals, as described above. These *in vitro* studies indicate that $C_{60}(OH)_{10}$/HP-β-CD can function as an effective antioxidative agent.

3.3. Protective effect of $C_{60}(OH)_{10}$/HP-β-CD nanoparticles on APAP overdose induced liver injury mice

$C_{60}(OH)_{10}$/HP-β-CD nanoparticles with a high radical scavenging ability were applied to the treatment of an APAP overdose induced liver injury, because various ROS such as the superoxide anion, hydroxyl radicals and peroxynitrite are significantly involved in this type of drug-injury. In this experiment, $C_{60}(OH)_{10}$/HP-β-CD nanoparticles were intraperitoneally administered to liver injured mice induced by the injection of an overdose of APAP. Serum ALT and AST levels were monitored in order to measure the level of the liver injury. As shown in Fig. 7, the serum ALT and AST levels of the mice were significantly increased to about 7000 ~ 13,000 IU/L as the result of the administration of a APAP overdose (400 mg/kg). A suspension of $C_{60}(OH)_{10}$ alone had no effect on those values. The administration of HP-β-CD alone had no effect on the increased serum AST and ALT levels, because it exerted no antioxidant effect (data not shown). In sharp contrast, $C_{60}(OH)_{10}$/HP-β-CD nanoparticles markedly suppressed those values. By the administration of 100 mg/kg $C_{60}(OH)_{10}$/HP-β-CD nanoparticles, the ALT and AST values were about 60 IU/L and 128 IU/L respectively, and the value was almost the same as those of normal mice (20–100 IU/L). 200 mg/kg of NAC was also intraperitoneally administered to the liver injury mice as a positive control. The AST (74 IU/L) and ALT (116 IU/L) levels were low as well as those in the case of the administration of $C_{60}(OH)_{10}$/HP-β-CD. The infiltration of inflammatory cells and bleeding were observed in cases of livers that had been treated with APAP (Fig. 7C). However, such damage was suppressed by the administration of $C_{60}(OH)_{10}$/HP-β-CD nanoparticles and NAC. Furthermore, $C_{60}(OH)_{10}$/HP-β-CD nanoparticles prolonged the survival rate of liver injured mice (Fig. 7C). About 80% of the mice treated with $C_{60}(OH)_{10}$/HP-β-CD nanoparticles survived for over 72 h, all of the mice that received no treatment died within 40 h. 85% of the mice treated with NAC survived for over 72 h. These results clearly indicate that $C_{60}(OH)_{10}$/HP-β-CD nanoparticles have a protective effect against the progression of liver injury induced by an overdose of APAP.

3.4. Changes in CYP2E1 expression and GSH level in liver

Liver injury is initiated by the formation of the reactive metabolite *N*-acetyl-*p*-benzoquinone imine (NAPQI), which is mainly

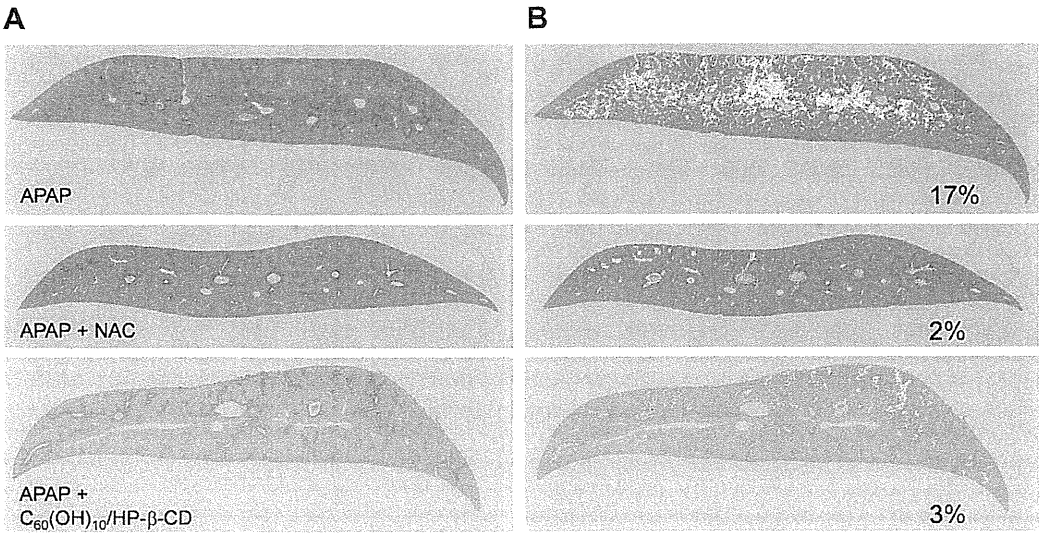

Fig. 9. Immunohistochemical staining of liver sections for nitrotyrosine protein adducts (A) and nitrotyrosine positive ratio in liver sections (B).

produced by CYP2E1 and results in the depletion of GSH. To better understand the mechanism associated with the protection of $C_{60}(OH)_{10}$/HP-β-CD nanoparticles, CYP2E1 expression and hepatic GSH levels were assessed. CYP2E1 activity was not affected by the administration of $C_{60}(OH)_{10}$/HP-β-CD nanoparticles, as shown in Fig. 8A. Hepatic GSH levels were significantly decreased after the injection of 400 mg/kg of APAP compared to the value for mice without APAP administration (Fig. 8B). Such GSH depletion was observed even in the case of the APAP plus $C_{60}(OH)_{10}$/HP-β-CD administration. The results indicate that $C_{60}(OH)_{10}$/HP-β-CD nanoparticles had no effect on CYP2E1 expression and GSH depletion.

3.5. *Effect of $C_{60}(OH)_{10}$/HP-β-CD nanoparticles against oxidative stress induced by APAP overdosed*

Peroxynitrite generation was visualized by immunohistochemical staining of liver sections for nitrotyrosine protein adducts. Livers were collected at 4 h after APAP administration. A significant number of hepatocytes were stained after an overdose of APAP and the entire liver section was stained (Fig. 9A). In contrast, in the case of the liver treated with $C_{60}(OH)_{10}$/HP-β-CD nanoparticles, the staining was limited to hepatocytes around the interlobular veins. The nitrotyrosine positive area for liver sections was calculated by based on microscopy observations (Fig. 9B). 17% of the area was stained in APAP overdosed liver sections, while the positive area was decreased to 3% by the administration of $C_{60}(OH)_{10}$/HP-β-CD nanoparticles, indicating that $C_{60}(OH)_{10}$/HP-β-CD nanoparticles protect liver from oxidative stress. The positive ratio was almost the same as 2% of NAC. The direct peroxynitrite scavenging ability of $C_{60}(OH)_{10}$/HP-β-CD nanoparticles was also examined (Fig. 10). The $C_{60}(OH)_{10}$ nanoparticles effectively scavenged peroxynitrite even at a low concentration and 80% of the peroxynitrite was scavenged by 10 μM of $C_{60}(OH)_{10}$ nanoparticles (Fig. 10A). Peroxynitrite is formed by the reaction between $O_2^{\bullet-}$ and NO, because of this, the scavenging activity of $C_{60}(OH)_{10}$/HP-β-CD nanoparticles against NO generated from SNP was studied. $C_{60}(OH)_{10}$/HP-β-CD nanoparticles showed scavenging ability for NO in a concentration dependent manner as shown in Fig. 10B. $C_{60}(OH)_{10}$/HP-β-CD nanoparticles had ability to suppress oxidative stress such as peroxynitrite and NO.

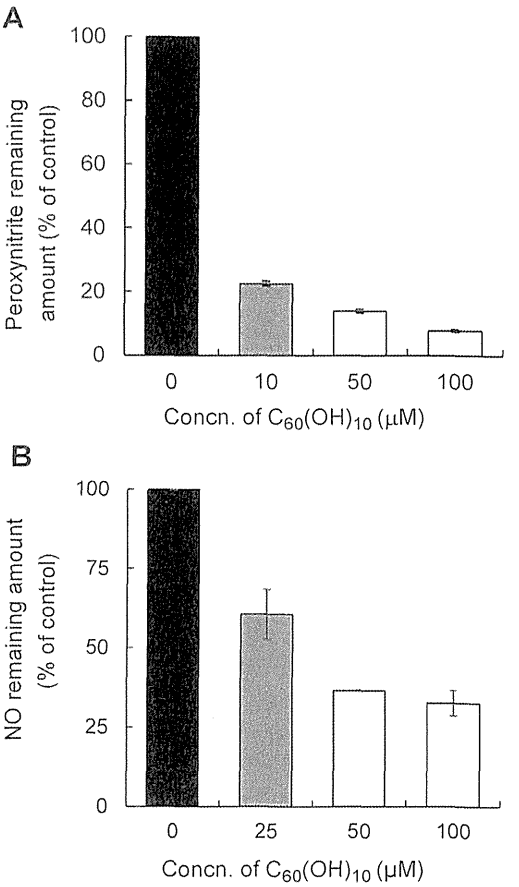

Fig. 10. Peroxynitrite (A) and NO (B) scavenging activity of $C_{60}(OH)_{10}$/HP-β-CD nanoparticles.

4. Discussion

Water soluble $C_{60}(OH)_{10}$ nanoparticles were prepared in high yields by grinding a mixture of HP-β-CD or γ-CD. On the other hand, α-CD and β-CD were less effective for solubilizing $C_{60}(OH)_{10}$ in water (Figs. 1 and 2). The resulting $C_{60}(OH)_{10}$/HP-β-CD and/γ-CD nanoparticles were stable in water for periods of over 1 month, and the initial small particle sizes of ca. 50 nm and 80 nm, respectively were retained (Fig. 4). A number of papers have reported that the large cavity of γ-CD is favorable for the inclusion of C_{60} and forms a water soluble inclusion complex [30,31]. On the other hand, α-CD and β-CD are thought to form a complex with more difficulty, because of the smaller cavity size. We previously reported that HP-β-CD and γ-CD are useful in terms of producing hydrophilic C_{60} nanoparticles in high yields and revealed that HP-β-CD can suppress the aggregation of the particles by covering the surface of the C_{60} nanoparticles through weak hydrophobic interactions and by physical adsorption [25]. It is likely that HP-β-CD and γ-CD would cover the surface of the $C_{60}(OH)_{10}$ nanoparticles in a manner similar to that for the C_{60}/CD systems. This surface covering of CDs on the $C_{60}(OH)_{10}$ nanoparticle is supported by a change in ζ-potential, as shown in Fig. 2B. The ζ-potential value reached a peak of −41 mv at a molar ratio of 1:1 ($C_{60}(OH)_{10}$:CD). However, it tended to increase positively with an increase in the molar ratio of CD from 1:1 to 1:5. The covering of the CDs shields the negative ζ-potential of the particles and shifts the potential in a positive direction, although the change is small. This hydrophilic layer of CDs formed on the $C_{60}(OH)_{10}$ nanoparticle surface, together with the large negative ζ-potential, prevents the particles from undergoing aggregation during storage.

The antioxidant ability of $C_{60}(OH)_{10}$/CDs nanoparticles were evaluated by scavenging studies using DPPH and ABTS radicals and ROS (Figs. 5 and 6). $C_{60}(OH)_{10}$/HP-β-CD and/γ-CD nanoparticles rapidly reacted with DPPH and ABTS radicals, compared with $C_{60}(OH)_{10}$ alone. HP-β-CD and γ-CD alone had no radical scavenging (data not shown). ESR spin-trapping studies using DMPO indicated that $C_{60}(OH)_{10}$/HP-β-CD and/γ-CD nanoparticles effectively scavenged ROS such as $O_2^{\bullet-}$ and •OH. The scavenging ability of $C_{60}(OH)_{10}$/HP-β-CD nanoparticles were higher than that of $C_{60}(OH)_{10}$/γ-CD nanoparticles, which may be due to the difference in surface areas between the HP-β-CD nanoparticles (46 nm) and the γ-CD nanoparticles (81 nm), i.e. the surface area involved in the scavenging is larger in the former particles than the latter particles. Therefore, stable hydrophilic $C_{60}(OH)_{10}$/HP-β-CD nanoparticles have the ability to act as a powerful antioxidant against, not only artificial free radicals, but also ROS that could affect biological systems.

$C_{60}(OH)_{10}$/HP-β-CD nanoparticles were administered to APAP induced liver injured mice (Fig. 7). The increment of serum ALT and AST levels was significantly suppressed, when $C_{60}(OH)_{10}$/HP-β-CD nanoparticles were administered. Survival rates were prolonged as the result of by the $C_{60}(OH)_{10}$/HP-β-CD administration, indicating that $C_{60}(OH)_{10}$/HP-β-CD nanoparticles have a hepatoprotective

effect. It has been reported that APAP induced liver injury is initiated by the production of the reactive metabolite, *N*-acetyl-*p*-benzoquinone imine (NAPQI) that is mainly produced by the enzyme CYP2E1. The metabolite, NAPQI is preferentially detoxified by hepatic glutathione (GSH). However, when the formation of NAPQI exceeds the capacity of GSH to eliminate NAPQI, GSH becomes depleted and NAPQI reacts with proteins, resulting in a selective oxidant stress and peroxynitrite formation in mitochondria [32]. Such an oxidant stress is responsible for mitochondrial DNA damage and the breakdown of the mitochondrial membrane potentials, which lead to necrotic cell death [33,34]. *N*-acetylcysteine (NAC), the only approved drug for the treatment of an APAP overdose, stimulates the synthesis of hepatic GSH, which supports the detoxification of NAPQI [35,36]. However CYP2E1 activity was not affected by the administration of $C_{60}(OH)_{10}$/HP-β-CD nanoparticles, as shown in Fig. 8A. Hepatic GSH levels were also decreased after the injection of APAP and (APAP + $C_{60}(OH)_{10}$/HP-β-CD) (Fig. 8B). Thus, CYP2E1 normally metabolizes APAP to NAPQI even in the case of the administration of $C_{60}(OH)_{10}$/HP-β-CD and the resulting overproduced NAPQI is consumed by GSH in hepatocytes. These results suggest that the protective effect of $C_{60}(OH)_{10}$/HP-β-CD against APAP induced liver injury cannot be explained in terms of changes in the production of NAPQI, an initiator of the APAP induced liver injury [37].

Peroxynitrite generation was evaluated by immunohistochemical staining liver sections for nitrotyrosine protein adducts (Fig. 9A). Entire liver sections were stained at 4 h after the APAP overdose. In contrast, the nitrotyrosine staining area was reduced by the treatment with $C_{60}(OH)_{10}$/HP-β-CD nanoparticles. The $C_{60}(OH)_{10}$ nanoparticles effectively scavenged peroxynitrite, even at a low concentration (Fig. 10A). The results indicate that $C_{60}(OH)_{10}$/HP-β-CD nanoparticles protect hepatocytes from oxidative stress, probably due to the scavenging of peroxynitrite. In addition to peroxynitrite, the $C_{60}(OH)_{10}$ nanoparticles also scavenged NO and $O_2^{\bullet-}$ in a concentration dependent manner (Figs. 6D and 10B). It is recognized that peroxynitrite is a critical mediator in the APAP overdose liver injury process [33] and is being mainly generated in hepatocytes [21,34]. Peroxynitrite is formed by a reaction between $O_2^{\bullet-}$ and NO inside mitochondria [34]. The findings reported herein reveal that $C_{60}(OH)_{10}$/HP-β-CD nanoparticles have the ability to scavenge, not only peroxynitrite, but also NO and $O_2^{\bullet-}$ (Figs. 6 and 10). Some C_{60} derivatives can permeate across the external cellular membrane and become preferentially localized in mitochondria [15,38,39]. Therefore, it is probable that $C_{60}(OH)_{10}$/HP-β-CD nanoparticles become localized in mitochondria after their administration and suppress oxidative stress by scavenging ROS such as $O_2^{\bullet-}$, NO and peroxynitrite, which act as critical mediators of such an injury (Fig. 11). A number of papers have reported that $C_{60}(OH)_{10}$ has a low biological activity and toxicity in biological media [9,15]. The above findings show that $C_{60}(OH)_{10}$ acquired a high ability for scavenging ROS and exerted a protective effect against liver injury by virtue of the formation of water soluble nanoparticles. The protective effect was almost the same as that of NAC, although the mechanism of liver protection is different in that NAC targets NAPQI while $C_{60}(OH)_{10}$ targets ROS. The combined administration of $C_{60}(OH)_{10}$/HP-β-CD and NAC might bring a synergetic effect in the treatment of APAP induced liver injury. $C_{60}(OH)_{10}$/HP-β-CD nanoparticles might be a potent antioxidant not only for the APAP overdosed liver injury but also for other diseases related to oxidative stress.

5. Conclusions

Stable hydrophilic $C_{60}(OH)_{10}$ nanoparticles were prepared by grinding with HP-β-CD. $C_{60}(OH)_{10}$/HP-β-CD nanoparticles were found to scavenge not only free radicals (DPPH and ABTS radicals) but also ROS ($O_2^{\bullet-}$ and •OH). By modifying the particles to acquire hydrophilic characteristics, they became more water soluble. In addition, the $C_{60}(OH)_{10}$/HP-β-CD nanoparticles were found to show a protective effect against APAP induced liver injury and the hepatoprotective effect of the nanoparticles is due to their ability to scavenge ROS such as $O_2^{\bullet-}$, NO and peroxynitrite. The developed $C_{60}(OH)_{10}$/HP-β-CD nanoparticles have the potential to serve as a new type of antioxidant and could be applied to other oxidative stress-related diseases.

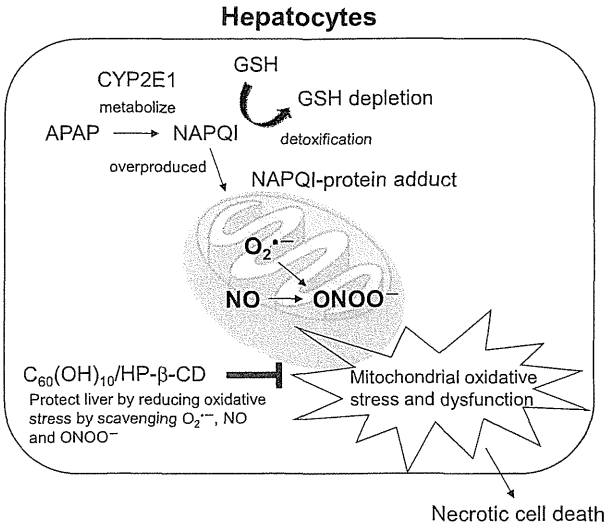

Fig. 11. Protective mechanism of $C_{60}(OH)_{10}$/HP-β-CD nanoparticles against APAP induced hepatotoxicity.

Acknowledgments

This work was partly supported by JSPS KAKENHI Grant Number 25860034. The authors are grateful to Ms. Fukuzawa and Ms. Fukudome for their technical assistance.

References

[1] Jensen AW, Wilson SR, Schuster DI. Biological applications of fullerenes. Bioorg Med Chem 1996;4:767–79.
[2] Bakry R, Vallant RM, Najam-ul-Haq M, Rainer M, Szabo Z, Huck CW, et al. Medicinal applications of fullerenes. Int J Nanomed 2007;2:639–49.
[3] McEwen CN, McKay RG, Larsen BS. C_{60} as a radical sponge. J Am Chem Soc 1992;114:4412–4.
[4] Markovic Z, Trajkovic V. Biomedical potential of the reactive oxygen species generation and quenching by fullerenes (C_{60}). Biomaterials 2008;29:3561–73.
[5] Maeda-Mamiya R, Noiri E, Isobe H, Nakanishi W, Okamoto K, Doi K, et al. In vivo gene delivery by cationic tetraamino fullerene. Proc Natl Acad Sci U. S. A 2010;107:5339–44. S/1–S/2.
[6] Zakharian TY, Seryshev A, Sitharaman B, Gilbert BE, Knight V, Wilson LJ. A Fullerene-paclitaxel chemotherapeutic: synthesis, characterization, and study of biological activity in tissue culture. J Am Chem Soc 2005;127:12508–9.
[7] Heymann D. Solubility of fullerenes C_{60} and C_{70} in seven normal alcohols and their deduced solubility in water. Fullerene Sci Technol 1996;4:509–15.
[8] Ruoff RS, Tse DS, Malhotra R, Lorents DC. Solubility of fullerene (C_{60}) in a variety of solvents. J Phys Chem 1993;97:3379–83.
[9] Eropkin MY, Melenevskaya EY, Nasonova KV, Bryazzhikova TS, Eropkina EM, Danilenko DM, et al. Synthesis and biological activity of fullerenols with various contents of hydroxyl groups. Pharm Chem J 2013;47:87–91.
[10] Fileti EE, Rivelino R, de Brito Mota F, Malaspina T. Effects of hydroxyl group distribution on the reactivity, stability and optical properties of fullerenols. Nanotechnology 2008;19:365703/1–365703/7.
[11] Jin H, Chen WQ, Tang XW, Chiang LY, Yang CY, Schloss JV, et al. Polyhydroxylated C_{60}, fullerenols, as glutamate receptor antagonists and neuroprotective agents. J Neurosci Res 2000;62:600–7.